



Vrije Universiteit Brussel

Faculty of Science & Bio-Engineering Sciences
Department of Physics

Bayesian evaluation of high-energy neutrino emission by Active Galactic Nuclei with the IceCube 40-string configuration

Proefschrift ingediend met het oog op het behalen van de graad van
“Master in de Wetenschappen”

Ben Dumoulin

Promotor: Prof. Dr. Nick van Eijndhoven

2011-2012



Acknowledgement

There are a lot of people I want to thank for this thesis. First of all I would like to thank Nick for his guidance, explanations and (extended) corrections to this thesis. Time is a valuable, non-renewable resource and I'm happy that he wanted to spend some of his time on me with this thesis.

Also I'm really happy I was made "part of the group" when I was working on this thesis in the IceCube group. Always having somebody available to disturb when I was stuck with something, saved me a lot of time and was way more fun than working on something alone.

In the beginning this were mainly Jan Kunnen and Mathieu Labare who I want to thank a lot for helping me out getting started. Later, in the analysis, I worked more closely with Debanjan Bose, Martin Casier and Lionel Brayeur which was not only fun, it helped me out a lot. I want to thank you for this guys.

The rest of the IceCube team I also thank for the nice coffee breaks and now and then the "beer breaks" at KK.

A very huge "thank you" goes to my parents who went through a lot of effort and gave me the opportunity to get me through my education. Thank you!

Samenvatting

IceCube is een neutrinotelescoop die op de Zuidpool gebouwd is. In essentie is het een rooster van Digitale Optische Modules (DOMs) in een ijsvolume van 1 km^3 . Het detecteert neutrino's indirect door de Cherenkovstraling te observeren van geproduceerde leptonen die gevormd worden wanneer een neutrino in het ijsvolume interageert. IceCube wordt geconfronteerd met een zeer hoog aantal achtergrondgebeurtenissen ("ruis") afkomstig van atmosferische muonen. Om gelijktijdig een maximaal aantal achtergrond events en een minimaal aantal signaal events te verwijderen, worden er een serie eventselecties toegepast. Deze worden besproken en de data set die hieruit resulteert is het startpunt van deze thesis.

Een voorafgaande studie heeft deze dataset geanalyseerd met een frequentistische methode om een significante flux van hoogenergetische astrofysische neutrino's te vinden. Deze was niet vastgesteld en dus heeft men een bovenlimiet op de sterkte van een mogelijk aanwezige signaalbron bepaald a.d.h.v. de Feldman-Cousins methode. In deze thesis analyseren we de dataset m.b.v. een Bayesiaanse methode voor een aantal specifieke mogelijke bronnen.

Eerst hebben we een bronstapelingsanalyse gedaan, die ons geloof in de mogelijke aanwezigheid van een bron kwantificeert. Deze analyse bestudeert gebieden rondom een set gekende bronnen; voor deze thesis bestaat die set uit 10 actieve kernen van sterrenstelsels (AGN) geselecteerd uit een online catalogus. We selecteren alle events uit onze dataset die binnen een 5° venster liggen van elk van de 10 afzonderlijke bronnen. Dan stapelen we de observaties van al deze bronnen op elkaar, hetgeen deze methode gevoeliger maakt voor zwakke signalen. We gebruiken de Bayesiaanse grootheid Ψ (die ons geloof in de aanwezigheid van een bron uitdrukt, gegeven de dataset) om uiteindelijk een p-waarde uit te rekenen. Deze p-waarde wordt berekend a.d.h.v. willekeurig gegenereerde gestapelde positie verdelingen, gebruik makend van de waargenomen gebeurtenissen. Dit levert een p-waarde van 0.87 op, hetgeen betekent dat 87% van de willekeurig gegenereerde verdelingen een grotere Ψ waarde hebben dan welke door ons is waargenomen. Hieruit kunnen we niet de aanwezigheid van een signaal concluderen.

We gaan dan verder door de 90% bovenlimiet op de bronsterkte te bepalen op een Bayesiaanse manier. Hierbij moeten twee prior waarschijnlijkheidsverdelingen (wdv) gekozen worden. Omdat anders de berekeningen te sterk gecompliceerd zouden worden, hebben we hier voor uniforme priors gekozen. We eindigen dan na wat rekenwerk met de wdv van de pure signaalrate, zonder achtergrond. Om alle grootheden te bepalen in deze wdv doen we twee experimenten (die gebruik maken van dezelfde dataset): we

kijken (in 5° vensters) naar de 10 AGN en we kijken (ook in 5° vensters) naar 10 achtergrondgebieden. Dit stelt ons in staat om onze daadwerkelijke meting te vergelijken met pure achtergrond en aldus de wdv voor een signaal te extraheren, welke we dan kunnen integreren tot de exacte waarde van de bovenlimiet die we wensen (i.e. geen “oversampling” zoals dat het geval kan zijn met de Feldman-Cousins methode). Dit resulteert in een bovenlimiet van $\Phi_{\nu_\mu}^{ul} = 11.64 \cdot 10^{-12} \text{ s}^{-1}\text{cm}^{-2}\text{sr}^{-1}$. Het resultaat dat uit de Bayesiaanse methode komt is in goede overeenstemming met de bovenlimiet van de flux bepaald via een vorige methode, $\Phi_{mean}^{ul} = 8.89 \cdot 10^{-12} \text{ s}^{-1}\text{cm}^{-2}\text{sr}^{-1}$.

Contents

1	Introduction	5
2	The Experimental Setup	9
2.1	Geometrical Layout	9
2.2	Event selection	15
3	Source Stacking Analysis	30
3.1	Bayesian degree of belief	30
3.2	Bayesian evaluation of histogram contents	32
3.3	The Ψ -analysis with IC-40 data	33
4	Bayesian Evaluation of the Astronomical Source Strength	37
4.1	The background rate pdf	39
4.2	On-source rate prior pdf	40
4.3	Determination of the source flux upper limit	43
5	Summary and outlook	47
5.1	Summary	47
5.2	Outlook	49

Chapter 1

Introduction

Since 100 years, the presence of cosmic rays is known. The study of these particles gave birth to the field of astroparticle physics. One of the questions right now is what the origin is of the highest energy particles (above 10^{18} eV) as shown in figure 1.1.

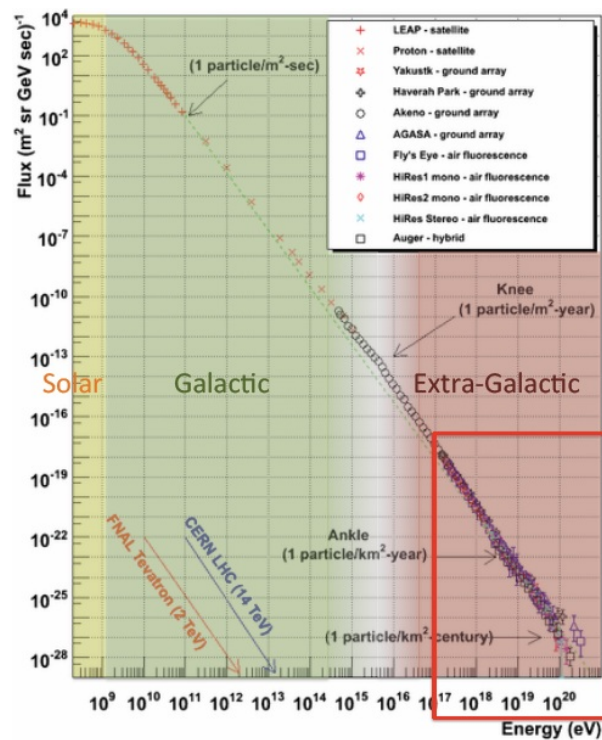


Figure 1.1: Spectrum of cosmic rays (courtesy W. Hanlon). Note: the indications of FNAL and LHC are incorrect

Candidate sources are sought after among the most violent phenomena in the universe, being Gamma Ray Bursts (GRBs) and Active Galactic Nuclei (AGN). These sources accelerate protons to very high energies which may form delta resonances when they interact with gamma rays. These delta resonances decay into pions and the charged pions subsequently decay into high-energy neutrinos as shown in figures 1.3 and 1.4. In the decay of the Δ -resonance into a nucleon and a π -meson, the meson obtains on average 20% of the primary proton energy. This yields an average neutrino energy of about 400 TeV for a primary proton energy of 10^{16} eV. An advantage of neutrinos is that they don't have a charge, so they don't interact with electric or magnetic fields on their way, which means they point straight to their source.

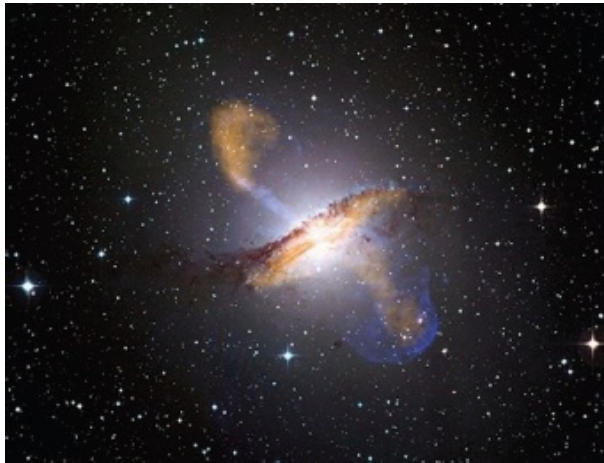


Figure 1.2: Relativistic particle outflow in the jets of an AGN

The latest experiment to study cosmic rays, specifically high-energy neutrinos, is IceCube [8]. Recently [1] it has been shown on the basis of IceCube measurements that GRBs cannot be the only sources of these very energetic cosmic rays. As such we will in this research focus on AGN and apply a novel statistical analysis method to search for neutrino signals associated with these objects. By stacking the observations of multiple sources, we achieve a high sensitivity for weak signals.

IceCube is confronted with a very high uniform background, coming from atmospheric interactions of cosmic rays. The data for this research are the IceCube 40 string configuration observations, which have been recorded between 2008 and 2009 and have been processed through the complete reconstruction chain, as outlined hereafter. A signal in this thesis is considered a

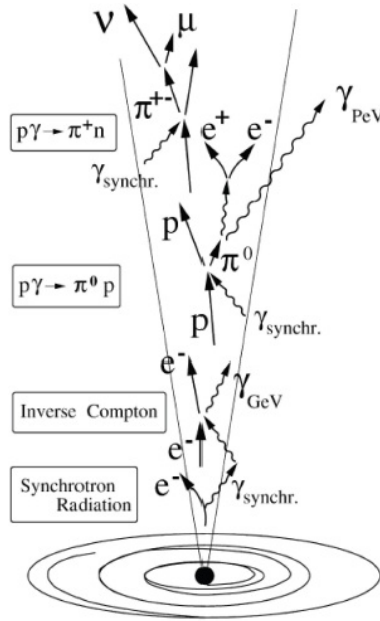


Figure 1.3: particle production in the relativistic jet of a cosmic accelerator

neutrino coming from an AGN. Out of these data, by means of a Bayesian method, we try to address the following questions:

- Can we identify a possible signal by our measurements?
- What is our degree of belief in the presence of a source?
- Can we determine the source strength or the limit on the source strength?

The performance of the IceCube detector and the processing of the recorded data from IC-40 will be discussed in the next chapter. In chapter 3 we outline a source stacking analysis on 10 selected blazars, to investigate the detectability of a source. With these same 10 sources we perform a Bayesian source strength analysis in chapter 4, followed by some conclusions and outlook for the future.

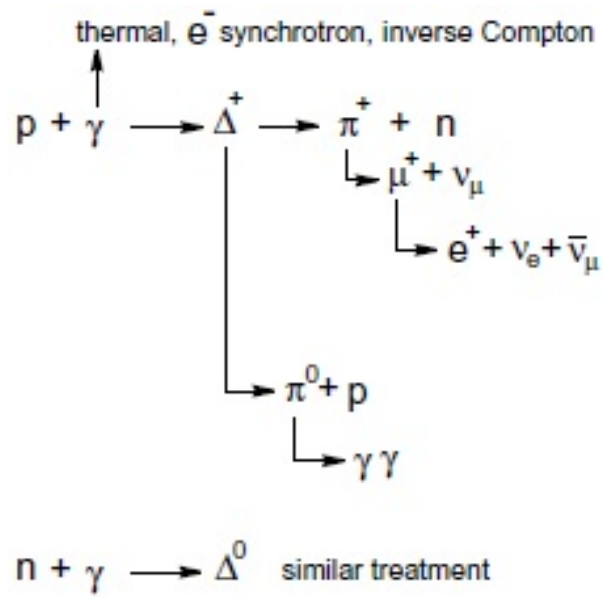


Figure 1.4: Neutrino production processes

Chapter 2

The Experimental Setup

2.1 Geometrical Layout

IceCube is a neutrino telescope, with the main scientific goal of mapping the high-energy neutrino sky [8]. The advantage of neutrinos for exploring the sky, is that they only interact weakly. This means that the neutrinos detected on earth have not been scattered on their path to us or directionally changed by the magnetic fields they encountered. So they will point straight to their source. However, this low interaction probability comes with a price: a very large and massive detector is needed.

High-energy neutrinos interact in this large volume according to the following reaction:

$$\nu_l + N \longrightarrow l + N \quad (2.1)$$

Where ν_l indicates a neutrino of type $l \in \{e, \mu, \tau\}$, N a nucleon and the corresponding charged lepton of type l . We will focus on the muon neutrino reaction. The produced muons will be nearly collinear with the ν_μ for high-energy neutrinos. They will be relativistic and produce Cherenkov radiation in the medium that they traverse. Huge water or ice volumes are the only practical candidates to realize a large transparent detector medium. The detector volume will be instrumented with photo-multiplier tubes (PMTs) to detect this radiation. A 1 km³ ice volume deep under the Antarctic surface was chosen, because of the extremely high transparency of these layers and the low background environment.

Cherenkov radiation is the electromagnetic radiation emitted by a charged particle that moves through a dielectric medium with a speed greater than the phase velocity of light in that medium (c/n , with n the refractive index of the medium and c the light speed in vacuum). The passing of a charged particle polarizes the atoms in that medium. The polarized atoms then rapidly turn

back to their original state, emitting EM radiation. It is analogous to an airplane breaking through the sound wall when moving faster than the speed of sound.

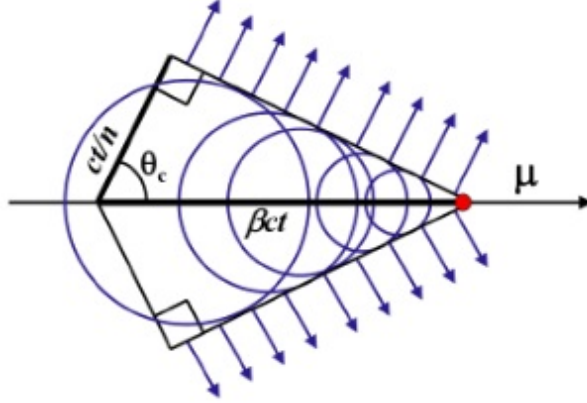


Figure 2.1: Illustration of the conical cherenkov radiation of a muon moving through a medium

While electrodynamics holds that the speed of light in vacuum is a universal constant (c), the speed at which light propagates in a material, c/n , may be significantly less than c .

In figure 2.1, a muon travels in a medium with speed v_μ such that $c/n < v_\mu < c$. We define the ratio between the speed of the particle and the speed of light as $\beta = v_\mu/c$. The emitted light waves (blue arrows) travel at speed $v_{em} = c/n$. The left corner of the triangle represents the location of the muon at some initial moment ($t=0$). The right corner of the triangle is the location of the muon at some later time t . In the given time t , the particle travels the distance

$$x_\mu = v_\mu t = \beta ct \quad (2.2)$$

whereas the emitted electromagnetic waves are restricted to travel the distance

$$x_{em} = v_{em} t = ct/n \quad (2.3)$$

So:

$$\cos(\theta_c) = \frac{1}{n\beta} \quad (2.4)$$

For high-energy muons $\beta \approx 1$ so that $\cos(\theta_c) \approx \frac{1}{n}$, which results in $\theta_c \approx 41^\circ$ in ice. This constant value of θ_c is used for the track reconstruction in IceCube, as outlined hereafter.

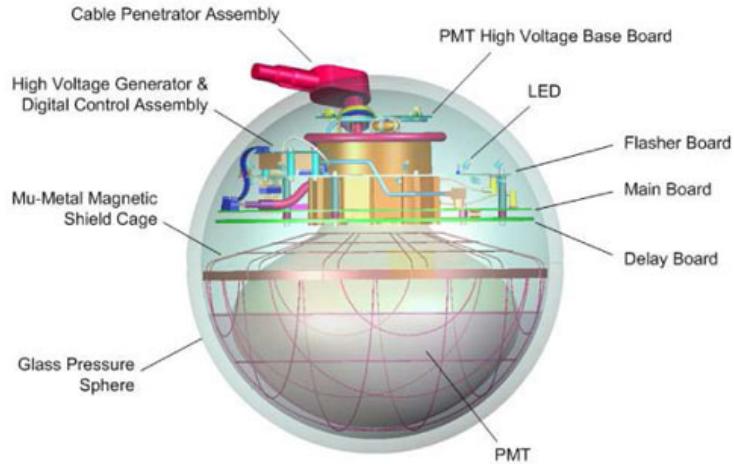


Figure 2.2: Schematic view of an IceCube DOM

IceCube consists of an array of Digital Optical Modules (DOMs). The purpose of a DOM is to detect, digitize and timestamp the signals from optical cherenkov photons. The digital output it produces is called a "hit". Figure 2.2 is a schematic view of a DOM, it's a 33.02 cm sphere containing a 25 cm PMT, a mu-metal magnetic shield and associated electronics responsible for the operation and control of the PMT as well as the amplification, digitisation and time-calibration. The Main Board (MB) is the "central processor" of the signal. When it receives an analog signal from the PMT, the signal is split in 3 parts. The first part goes to a trigger. The second part goes through a 75 ns delay line and is then split again over 3 channels of the two Analog Transient Waveform Discriminators (ATWDs), designed for high-bandwidth waveform capture. Each of these channels has a different amplification in order to obtain a large dynamic range. The third part goes to a FADC (Fast Analog to Digital Converter) designed for handling longer signals at a lower sampling speed [7].

The IceCube Neutrino Observatory is a 1 km³ detector built in the Antarctic ice, in a 1450-2450 m deep layer and an air shower detector (IceTop) at the surface. Actually the detector consists of 3 cooperating components: the IceCube in-ice Array, DeepCore and IceTop. The geometry shown in figure 2.3 has been optimized using benchmark fluxes and detailed detector simulations [8].

- IceCube Array: 4680 DOMs make up the main in-ice array. They are deployed vertically over 78 strings with 60 DOMs per string. The

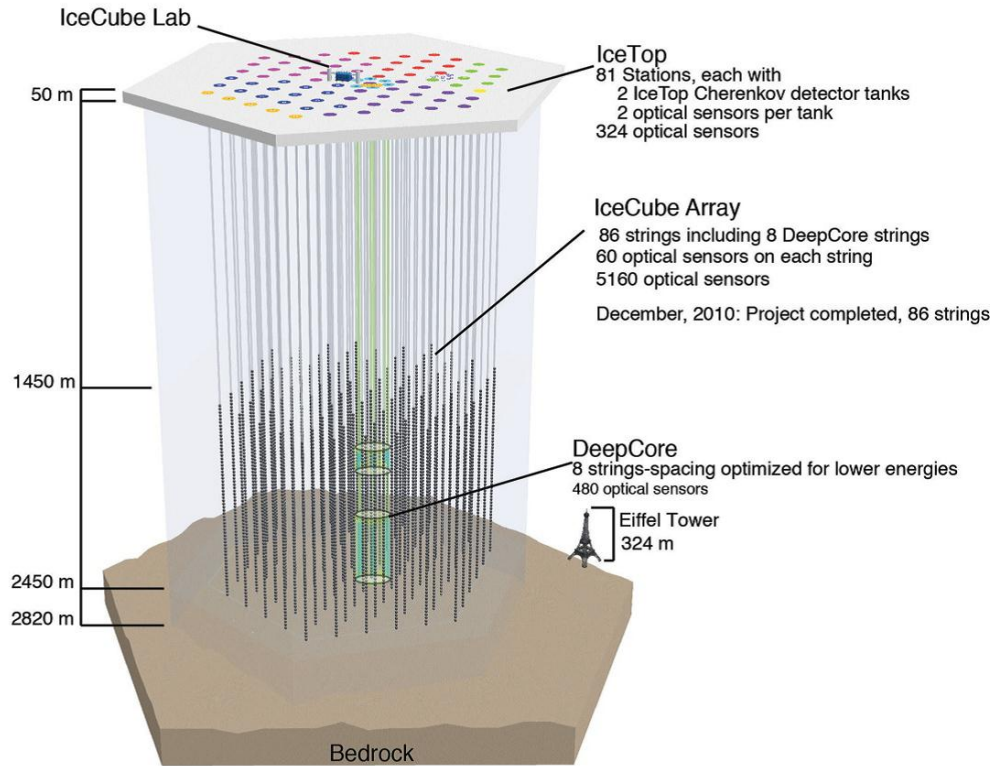


Figure 2.3: View of the IceCube detector layout with the 3 separate components indicated. The data used in this thesis come from the 40 string configuration, which is half of the completed in-ice array (without DeepCore)

vertical spacing between each DOM is 17m and the horizontal spacing between each string is 125m. The design is optimized for energies in the TeV-PeV range. The strings form a hexagonal pattern.

- DeepCore is an extension of the in-ice array and is deployed within the main in-ice array. The DeepCore DOMs are located where they can benefit from the ice layers with optimal clarity (measured by the dust concentration). In the 2107-2450m layer there are 50 DOMs per string, with a vertical spacing of 7m. In the 1750-1860m layer there are an additional 10 DOMs per string with a 10 m vertical spacing. DeepCore consists of 8 specialized strings which in total lower the energy threshold to about 10 GeV which is a large improvement compared to the

about 200 GeV threshold of the standard IceCube array. The DeepCore strings are located in between the regular IceCube strings, so that an interstring-spacing of 72 m is achieved. Together with the seven adjacent standard IceCube strings these 8 strings form the DeepCore array in the center of IceCube.

DeepCore is located at the center of IceCube in the deepest part of the south pole, so the surrounding IceCube DOMs can serve as a veto. Atmospheric muons will induce signals in the surrounding IceCube sensors before they reach the DeepCore DOMs. A neutrino that interacts in the DeepCore region may produce a muon that reaches the surrounding IceCube region, but the IceCube sensors will be activated at a later time than the DeepCore ones. A veto region has been defined and an event that triggers DOMs in this veto region before hitting DOMs in the DeepCore region are treated as atmospheric background.

- IceTop: the largest contribution of background events comes from cosmic air showers. An array of DOMs located at the surface, called IceTop, will measure these air showers. It consists of 81 stations located at the IceCube string positions. Each station contains 2 ice tanks with a 1m radius and 90cm deep ice. Each tank contains 2 DOMs and the tanks are separated 10m from each other and the corresponding IceCube string. In total IceTop consists of 324 DOMs. IceTop is able to measure the cosmic ray spectrum and composition between 10^{14} and 10^{18} eV.

At depths lower than 1450m, the Antarctic ice is free of air bubbles and exhibits an exceptional optical clarity. The depth and wavelength dependence of the scattering and absorption have been measured with a variety of in-situ light sources. Recently the ice properties have been measured over the full depth range of the IceCube detector using the in-situ LEDs present in every DOM main board resulting in what is called the South Pole Ice(SPICE) model [9]. Figure 2.4 shows the absorption and scattering profile of the second iteration of SPICE, *SPICE*² ("spicetwo"), which uses the dust logger and ice core data to extrapolate the ice properties to the region outside the detector volume.

For relativistic muons formula (2.4) can be used for the reconstruction of the track. Because the muon is relativistic, $\beta \approx 1$ and n is determined by the material. For ice $n \approx 1.32$, so $\theta_c \approx 41^\circ$. In case a set of DOMs is triggered and the arrival times and amplitudes of the signals are registered, this information, together with the locations of the DOMs, can be used [12] to develop a maximum likelihood method for reconstruction of the corresponding track

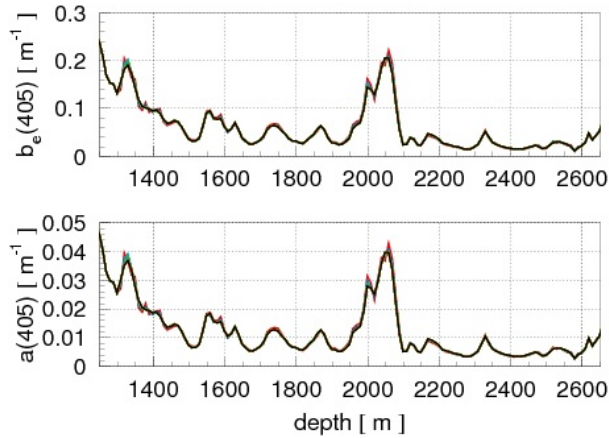


Figure 2.4: The profile of the absorption (lower panel) and scattering (upper panel) coefficient resulting from the *SPICE*² measurements at 405 nm average flasher wavelength

parameters. Given a hypothetical track, its likelihood can be calculated and as such the most likely track can be found via well-established minimization algorithms [13]. The likelihood method is performed in two steps. First, online, a single photoelectron (SPE) method is performed. This procedure only uses the arrival time of the first photon in each DOM. Later, offline, a more sophisticated likelihood method is performed, the multiple photoelectron (MPE) likelihood method. This algorithm uses the arrival times of the first N expected photons and takes into account that the first photon is on average less scattered than the next ones. This method improves the directional information from the data. The likelihood reconstructions need an initial track hypothesis to start the optimization. The initial track is derived from first guess methods, which are fast analytic algorithms that do not require an initial track hypothesis [10].

The IceCube coordinate frame is different from the declination/right ascension frame, which is shown in figure 2.5. IceCube uses a horizontal detector frame with the center of IceCube at its origin. The x axis points to the East, the y -axis to the North and the z -axis to the zenith such that the z -axis and the Earth's rotation axis are aligned, which yields a simple transformation to equatorial coordinates. Furthermore, due to the polar location of the detector, objects with a certain declination will be observed at a fixed zenith angle. This enables observations over long exposure times with minimal systematics due to zenith angle dependent reconstruction efficiencies.

Radiative energy loss processes generate secondary charged particles along

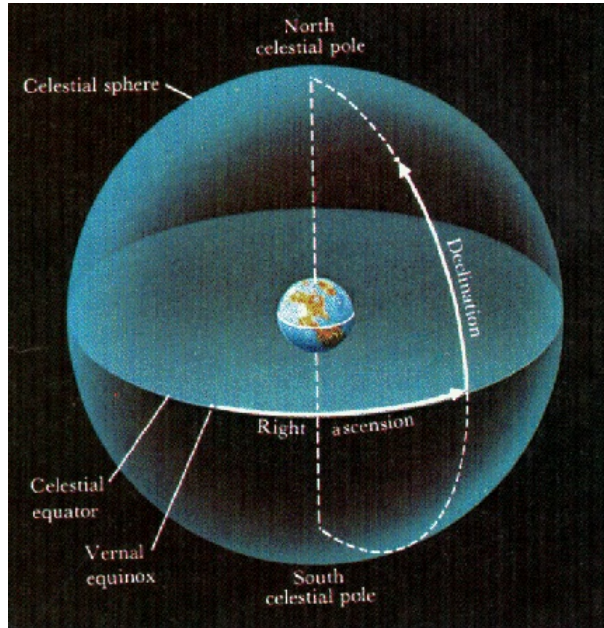


Figure 2.5: The traditional declination-right ascension frame

the muon trajectory, which also produce Cherenkov radiation. These additional photons allow an estimate of the muon energy. The resolution of this method is limited by fluctuations in these processes. Since the estimate is performed for the muon energy, it provides a lower bound for the initial neutrino energy. This energy estimate is heavily used in a search for a diffuse cosmic neutrino flux. It is used to separate a possible signal from the atmospheric background by selecting a minimum energy based on their different energy dependencies ($E^{-2.7}$ for atmospheric background, E^{-2} for signal). This minimum energy is exactly what the lower bound energy provides us with. However, in the current analysis we have other means to reduce the background as explained hereafter, so we will not make use of the energy estimate in order to minimize the bias in our event sample.

The recorded events after track reconstruction are still strongly dominated by atmospheric muons. To reduce this background, a set of selection criteria are applied. These cuts are the content of the next section.

2.2 Event selection

The main trigger for the data considered here was a multiplicity condition which required 8 DOMs to exceed their discriminator threshold within a 5

μs time window. This $5 \mu\text{s}$ comes from IceCube’s 1 km^3 volume. The largest distance a particle can travel in a straight line in a cube with sides of 1 km is $\sqrt{3} \text{ km}$. It takes light around $5 \mu\text{s}$ to cross this distance. In addition, a local coincidence condition was enforced that requires the vertical neighbors of the triggered DOMs to trigger within $1 \mu\text{s}$ of each other.

In a subsequent step the triggered data are filtered. The purpose is to apply filtering criteria to separate high-energy neutrinos from mis-reconstructed atmospheric muons and to mark events which are of interest for the different (astro)physics analyses. Filter criteria to perform a first event classification (e.g. track or cascade like) based on fast reconstruction results are performed online at the South Pole and form the so-called level 1 (L1) filtering, to select the events to be directly sent north via satellite connection for further processing offline. The selection criteria that are used on the IC-40 data in the current analysis, are summarized in Table 2.1 and discussed below. Table 2.2 summarizes the number of selected events after each cut.

Background events, which pass a zenith angle selection as outlined below, need to be rejected by applying selection criteria on quality parameters. These parameters usually evaluate information, which is not optimally exploited in the reconstruction. The detailed choice of quality parameters is specific to each analysis. Below we discuss the quality parameters used to obtain the final analysis sample for the current analysis and the selection criteria we applied on them.

The effects of the various selections on both the data and simulated signal and background samples are reflected in table 2.2, whereas the selections together with the final data sample are shown graphically in figures 2.6-2.13. The simulated samples represent the live time of the data set of the current analysis. The signal simulation was performed for the generic benchmark flux [8] $E^2 \frac{dN}{dE} = 10^{-7} \text{ GeV cm}^{-2} \text{ s}^{-1} \text{ sr}^{-1}$.

1. **Reconstructed zenith angle (θ):** zenith angles above 90 degrees are selected because the particles corresponding to these tracks have passed through the earth and in this way the earth is used as a filter to reduce the background from atmospheric air showers, since only neutrinos are able to traverse the Earth. These tracks are called “upgoing”
2. **Reduced log likelihood (the log-likelihood divided by the number of degrees of freedom):** a small value of the log-likelihood indicates that the Cherenkov photons arrived at the individual DOMs consistent with the likelihood description of photon arrival times [12]. As such, well reconstructed tracks may be selected for the final analysis. The cut values are determined from figure 2.6. The green line

indicates the expected atmospheric neutrinos and the dots indicate the data. The observable N_{Ch} indicates the number of DOMs that fired in the corresponding event and $N_{Ch}-5$ represents the number of degrees of freedom for a track fit. Above $\frac{\log(L)}{N_{Ch}-5} = 8$, a considerable fraction of the data events is not passing a Bayesian selection (see later) and are compatible with atmospheric muons. These events are removed from the sample by only retaining the events with a reduced log likelihood value below 8. In the lower plot of figure 2.6, a slightly more strict selection is shown for which the events below the cut-value $\frac{\log(L)}{N_{Ch}-2.5} = 7.1$ are kept; the ones above this value are not retained. For our analysis we use a logical OR of both selections.

3. **Error estimate for the MPE reconstruction (σ):** the directional error ellipse, with $\sigma = \sqrt{\sigma_x^2 + \sigma_y^2}$, for the MPE log-likelihood reconstruction represents the angular resolution of the reconstructed tracks. It is estimated by calculating an optimized confidence ellipse [11]. Its value is particularly important for localized searches as the one in this thesis and the distribution is shown in figure 2.7. For σ above $\approx 2^\circ$ the data points start to deviate further from the expected curve (in green) and their uncertainty starts to grow. As a compromise between retaining signal events and removing badly reconstructed tracks, the cut value has been put at 3° , the data below are kept as seen in figure 2.7.
4. **Minimum zenith angle of a two-muon reconstruction**
($\theta_{SplitGeo, SplitTime}$): a substantial fraction (see table 2.2) of the atmospheric muon background results from two or more muons triggering the IceCube detector during the trigger time window. Some of these coincident downgoing muon events might mimic an upgoing event. The purpose of this cut is to reduce this background source. Consider a set of DOMs that have been triggered within a single time window and a single track is reconstructed. Subsequently the set of triggered DOMs is split into two groups and each group is used to reconstruct a muon track. The separation is accomplished in two ways. The first, $\theta_{SplitGeo}$, uses a geometric approach by constructing a plane perpendicular to the MPE-reconstructed track to equally divide the hit positions. The second, $\theta_{SplitTime}$, is performed temporally by using the mean Cherenkov photon arrival time as a separator. After yielding two separate tracks by reconstruction of the two different sets of hits, this cut requires both of these tracks to have a zenith angle bigger than 80° , as seen in figure 2.8, which means the event is not compatible with downgoing

atmospheric muons which mimic an upgoing muon.

5. **Log-likelihood ratio between a zenith-weighted Bayesian reconstruction and a standard reconstruction:** The Bayesian likelihood ratio (see section 3.1) compares the hypothesis of an up-going muon track with the alternative hypothesis of a downgoing track, given the prior information about the zenith-dependent flux of (downgoing) atmospheric muons w.r.t. atmospheric (upgoing) neutrinos. The Bayesian likelihood reconstruction is performed by minimizing the product of the standard likelihood and the Bayesian prior (concerning the zenith-dependence of the atmospheric muons). The lowest values of the log-likelihood ratio support the alternative hypothesis of a down-going muon, whereas higher values indicate an up-going muon track. The likelihood ratio is zenith angle dependent and thus the selection criterion based on $\log(L_{\text{Bayes}}/L)$ varies with the zenith-angle of the MPE reconstructed track, as indicated in table 2.1. Figure 2.9 shows the accepted and rejected events where a threshold of $\log(\frac{L_{\text{Bayes}}}{L}) > 25$ has been used for upgoing candidates.

6. **Log-likelihood ratio between a zenith-weighted two-muon Bayesian reconstruction and a standard reconstruction:** The two-muon Bayesian likelihood ratio compares the hypothesis of a single up-going muon track with the alternative hypothesis of two down-going muon tracks, while using the prior information about the known zenith-dependent flux of atmospheric (downgoing) muons like before. The two down-going muons were reconstructed separately using the DOM splitting strategies as above: yielding L_{Bayes1} and L_{Bayes2} , respectively. Each muon is reconstructed with a Bayesian prior defined with a zenith-dependent weight of the downgoing atmospheric muon flux. This observable is constructed to reject misreconstructed coincident atmospheric muons. As in the single muon case above, low values support the alternative hypothesis of two down-going muons whereas higher values indicate an up-going muon track. As seen in figure 2.10, $\log(\frac{L_{\text{Bayes1}}+L_{\text{Bayes2}}}{L})$ is required to be bigger than 35.

7. **Number of DOMs with direct photoelectrons (NDir):**
 Unscattered Cherenkov photons provide the best information for the reconstruction and thus is the quality of a reconstructed track proportional to the number of direct photons. NDir is defined as the number of hits with small time residuals: $t_1 < t_{\text{res}} < t_2$, where the time residual, t_{res} , is the difference between the observed hit time and the hit

time expected for a direct photon ($t_{res} \equiv t_{hit} - t_{geo}$) [12]. Which values for t_1 and t_2 are used depends on the type of analysis, here $t_1 = -15$ ns and $t_2 = 75$ ns. The NDir distribution is shown in figure 2.11, along with the cut $NDir > 5$.

8. **Direct length of the reconstructed track (LDir):**

The set of direct photon hits can be projected on the reconstructed track. The distance between the two outer most points gives LDir. The longer this distance is, the more robust and precise the reconstruction of the track direction is. The LDir distribution is given in figure 2.12. The events below 240 m are rejected retaining only the events that provide enough lever arm for a good track reconstruction.

9. **Smoothness of the reconstructed track (SDirC):** The track reconstruction methods consider the pdf for each hit separately but ignore the correlations. Therefore, the reconstruction can assign the same likelihood to tracks where most of the hits cluster at one end of the reconstructed track and tracks where the same number of hits are smoothly distributed along the track. Because of the hypothesis of constant light emission by a muon along its track, high quality reconstructions have equally spaced hits. SDirC is a measurement of how uniformly the projected direct photons are along the reconstructed track:

$$SDir_j \equiv \frac{j-1}{N-1} - \frac{l_j}{l_N}, \quad (2.5)$$

$$SDirC \equiv \sum_{j=1}^N SDir_j \quad (2.6)$$

Where l_j is the distance along the track between the points of closest approach of the track to the first and the j th hit module, with the hits taken in order of their projected position on the track and N the total number of hits. In this way SDirC is confined between -1 and 1. Positive values indicate that the photons cluster at the beginning of the track. Negative values indicate they are more located at the end of the track. A smoothness that is close to 0 indicates a uniform distribution of projected Cherenkov photons. The acceptance region for events is $-0.52 < SDirC < 0.52$ as shown in figure 2.13.

After all these cuts have been applied, there are 12,877 candidate events left as seen in table 2.2. Note that the final data sample represents events in the full Northern hemishpere. In our analysis (see hereafter) we will select

Cut	Selection criterium
1	$\theta > 90^\circ$
2	$\frac{\log(L)}{n_{ch}-5} < 8$ OR $\frac{\log L}{N_{ch}-2.5} < 7.1$
3	$\sigma < 3^\circ$
4	$\theta_{SplitTime} > 80^\circ$ $\theta_{SplitGeo} > 80^\circ$
5	$\log(L_{Bayes}/L) > 25$ FOR $\cos(\theta) < -0.2$ $\log(L_{Bayes}/L) > (75\cos(\theta) + 40)$ FOR $\cos(\theta) > -0.2$
6	$\log\left(\frac{L_{Bayes1}+L_{Bayes2}}{L}\right) > 35$
7	$NDir > 5$
8	$LDir > 240$ m
9	$ SDirC < 0.52$

Table 2.1: Summary of the selection criteria that were discussed above

only patches of 5° around possible sources, which will reduce the background by an additional factor of about 0.0038 whereas basically all signal events will be maintained. These events agree very well with the atmospheric neutrino flux (see figures 2.6-2.13) and form the starting point of the analysis described in this thesis. The zenith distribution at the final analysis level is shown in figure 2.14.

The atmospheric neutrinos are expected to fall in uniformly from all over the sky. The declination distribution of the events in our sample is shown on the left hand side of figure 2.15. The observation that there are more events for lower declination is due to a geometrical effect. Consider a sphere around the earth with declination bands of 1 degree. The surface in such a band, when you integrate over the right ascension, is plotted in the right hand side of figure 2.15.

In polar coordinates (θ, φ) , a θ distribution of uniform events follows a cosine. At a sphere the surface between $(0,1)$ degrees (top of the sphere) in θ is smaller than the surface formed between $(89,90)$ degrees (equator of the sphere). Since the surface is bigger, there will be more events recorded in the equator band in a uniform distribution. To give this an exact expression we integrate a surface over 360 degrees in azimuth φ :

$$d\Omega = \sin(\theta)d\theta d\varphi \quad (2.7)$$

$$\Omega_{\text{band}} = \int_0^{2\pi} \int_0^{\delta} \sin(\theta)d\theta d\varphi = 2\pi \sin(\theta)d\theta = -2\pi d[\cos(\theta)] \quad (2.8)$$

This solid angle distribution is shown on the right hand side of figure 2.15. Since $\delta = 90^\circ - \theta$ the declination band distribution follows a sine.

Purity Criterion	Data	Total Atm. μ	Coincident μ	Atm. ν_μ	$E^{-2}\nu_\mu$
Triggered	3.3×10^{10}	2.98×10^{10}	1.72×10^{10}	1×10^6	1.03×10^4
L1 Filter	8.0×10^8	7.5×10^8	3.9×10^8	1.14×10^5	1,956
θ	2.4×10^8	3.0×10^8	1.79×10^8	91,246	1,353
$\log(L)$	8.46×10^6	4.58×10^6	1.12×10^6	43,183	934
σ	1.43×10^6	1.05×10^6	4.1×10^5	37,174	677
$\log(L_{Bayes}/L)$	2.88×10^5	2.73×10^5	2.36×10^5	27,411	659
$\log(\frac{L_{Bayes1}+L_{Bayes2}}{L})$	44,309	24,032	17,648	18,400	622
$\theta_{SplitTime}$	22,154	3,004	2,253	15,771	556
$\theta_{SplitGeo}$	17,648	1,126	751	15,020	532
NDir	15,771	751	370	14,645	524
LDir	13,518	374	325	14,269	499
SDir	12,877	4	0	13,466	475

Table 2.2: The number of selected events after each cut for data and simulation for atmospheric muons, conventional atmospheric ν_μ and E^{-2} astrophysical ν_μ with a standard benchmark flux of $E^2 \frac{dN}{dE} = 10^{-7} \text{ GeV cm}^{-2} \text{ s}^{-1} \text{ sr}^{-1}$

$$S[\delta, \delta + d\delta] = 2\pi \cos(\delta) d\delta = 2\pi d[\sin(\delta)] \quad (2.9)$$

The sine of the declination should be a uniform distribution as indicated before, since it takes the geometrical effect into account. The declination distribution is shown in figure 2.16. At low declinations some irregularity is observed due to less accurate reconstruction of (nearly) horizontal tracks.

Our selection criteria (e.g. LDir) indirectly affect the energy threshold. In figure 2.17 the energy distribution of our event sample is presented, showing that we have good sensitivity above about 1 TeV.

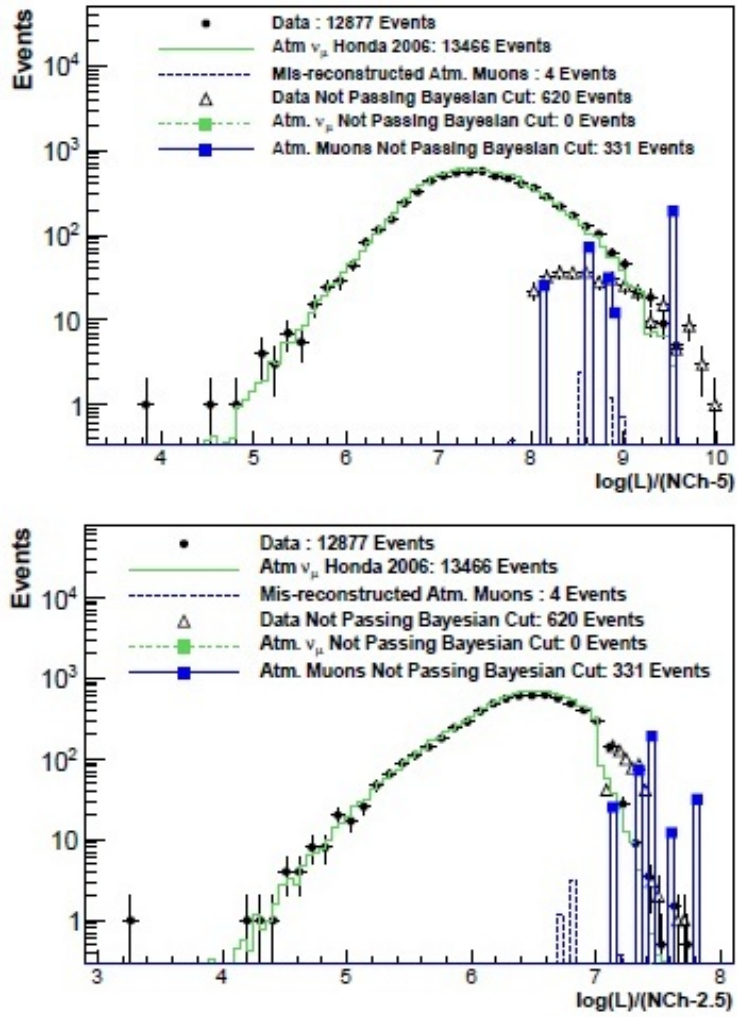


Figure 2.6: Reduced log-likelihood distributions. The lower plot shows a more strict selection of the reduced log-likelihood

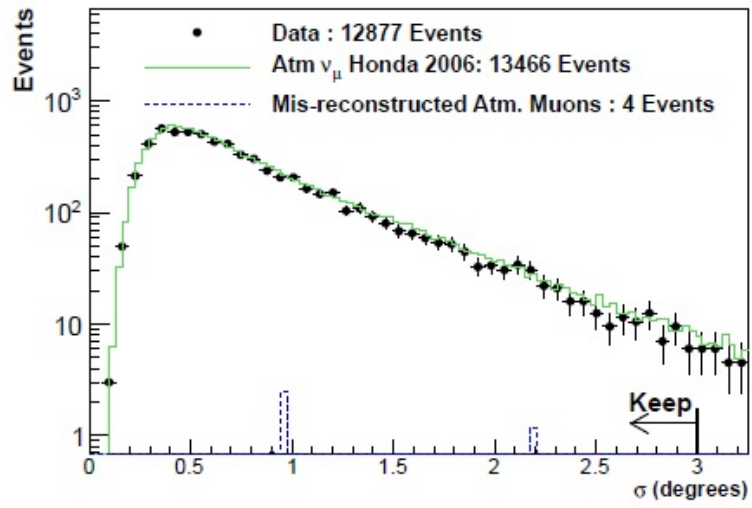


Figure 2.7: Distribution of the reconstructed angular uncertainty (σ) for an atmospheric neutrino spectrum, the data and misreconstructed atmospheric muons

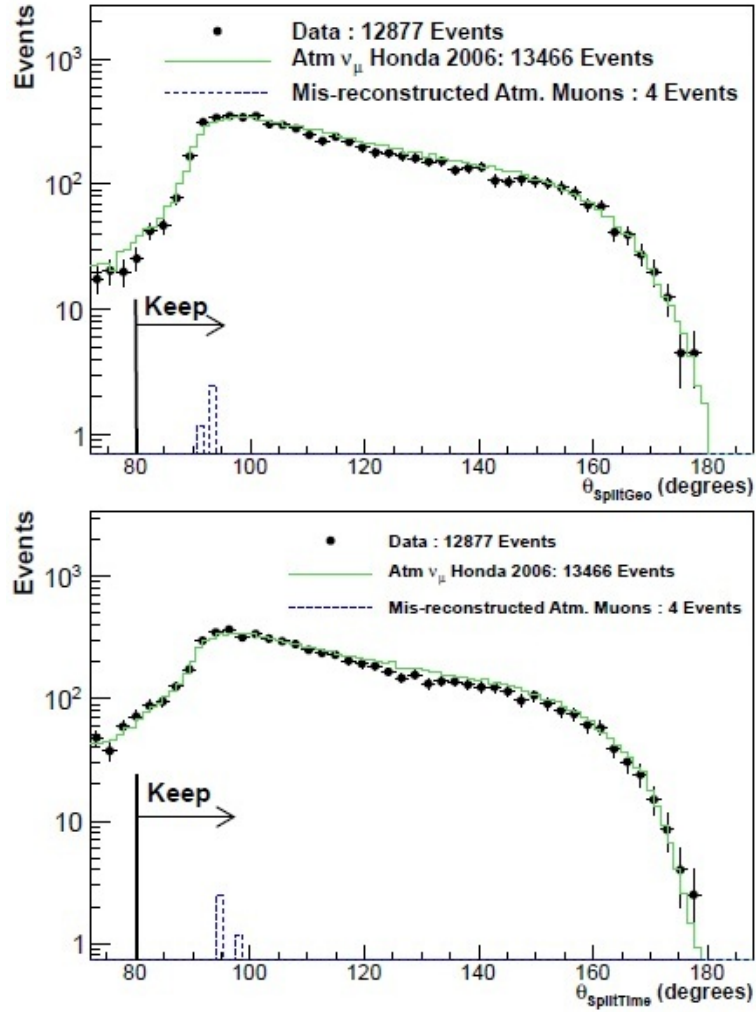


Figure 2.8: The SplitGeo (top) and SplitTime (bottom) angular distributions. The dots indicate the data, the green lines indicate the expected atmospheric neutrino distribution and the dotted line represents the mis-reconstructed atmospheric muons. The events to the right of the black line are retained. For further details see the text.

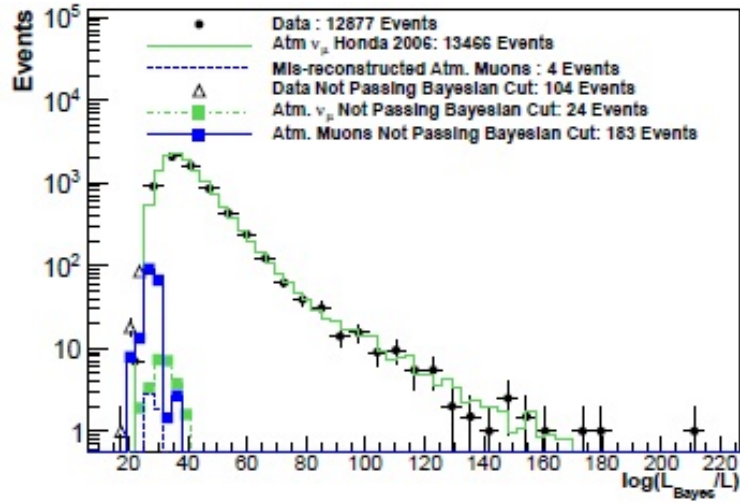


Figure 2.9: The distribution of the log-likelihood ratio of a zenith-weighted Bayesian reconstruction and a standard reconstruction for atmospheric neutrinos and the data. Events with $\log(L_{Bayes}/L) > 25$ are retained. The events that did not pass the cut and their nature are also shown.

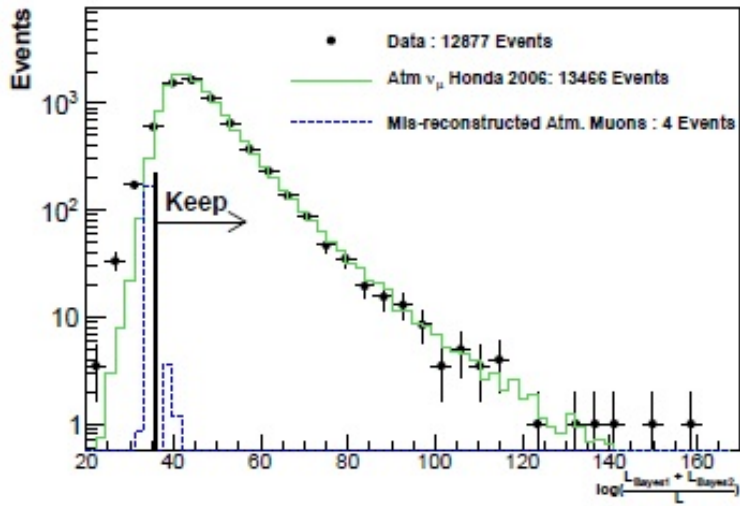


Figure 2.10: The distribution of the log-likelihood ratio of a zenith-weighted two-muon Bayesian reconstruction and a standard reconstruction for atmospheric neutrino, data and mis-reconstructed atmospheric muons. The applied cut is shown to be at a value of 35.

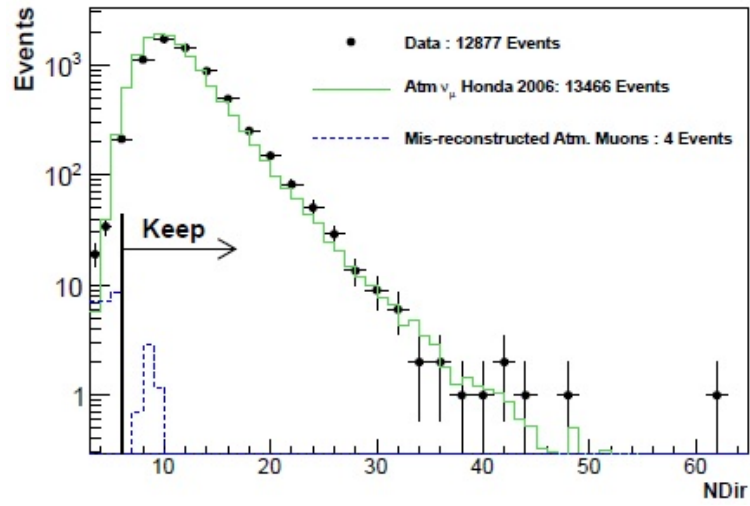


Figure 2.11: Distribution of the number of direct hits.

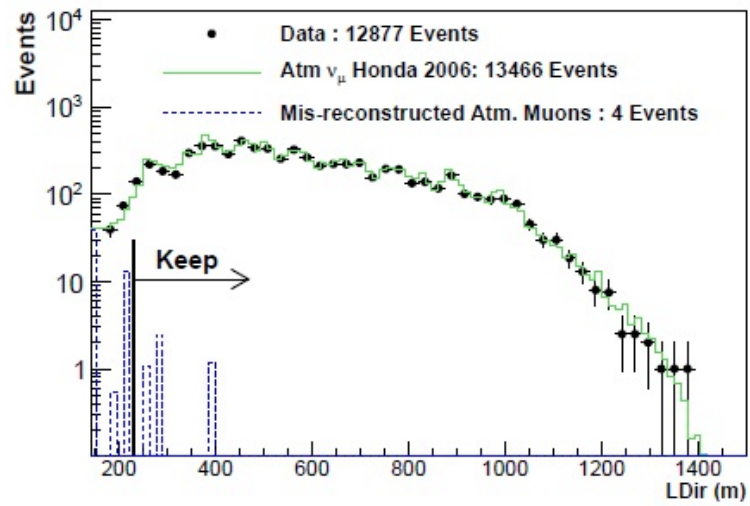


Figure 2.12: Distribution of the direct track length.

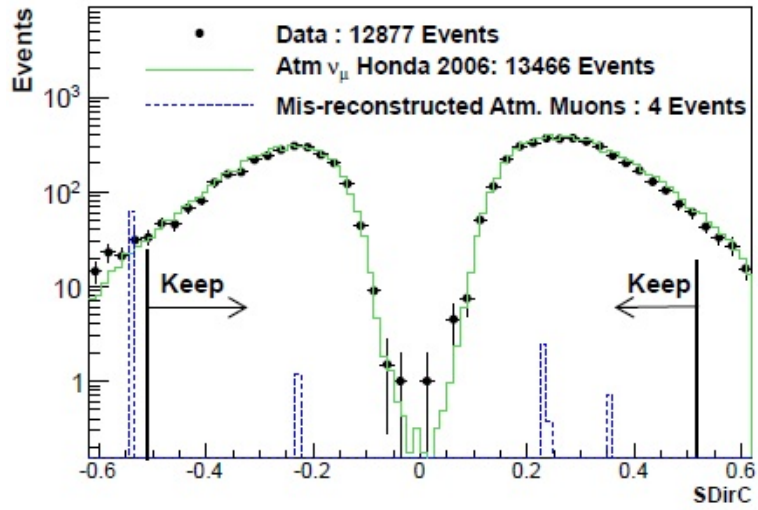


Figure 2.13: Distribution of the track smoothness.

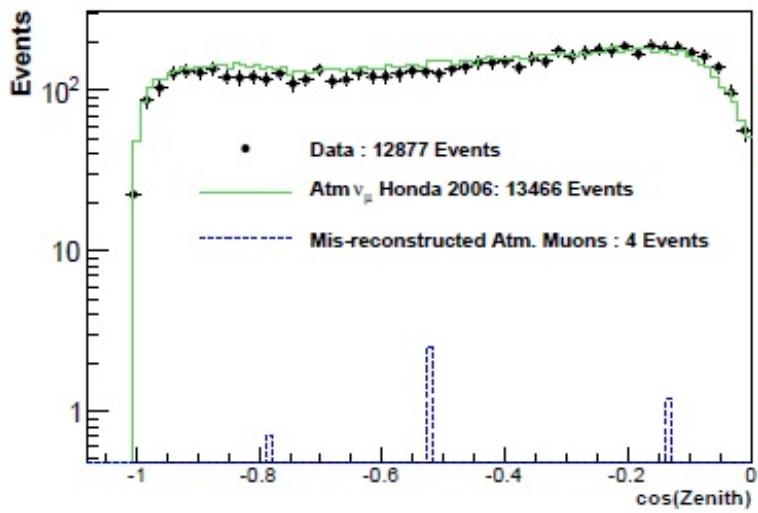


Figure 2.14: The zenith angle distribution at final analysis level for the data (black) and atmospheric neutrino Monte Carlo (green)

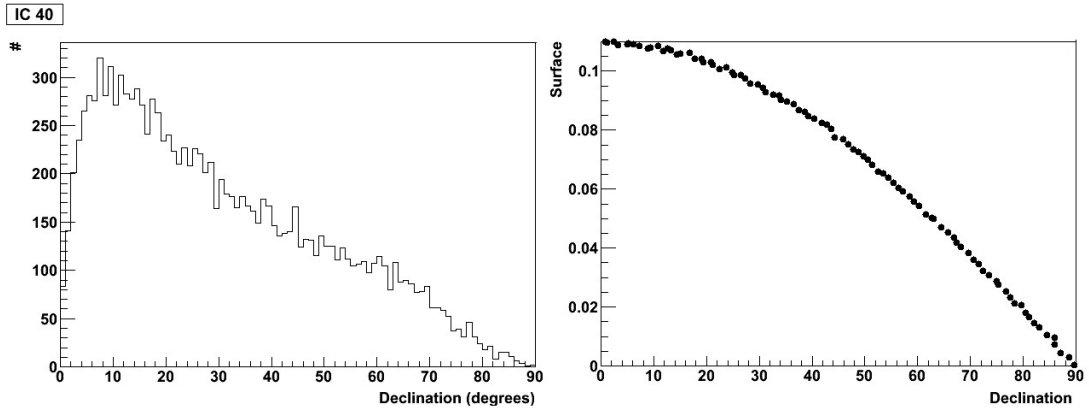


Figure 2.15: Declination distribution (left) and integrated declination band (right) distribution to show the solid angle effect

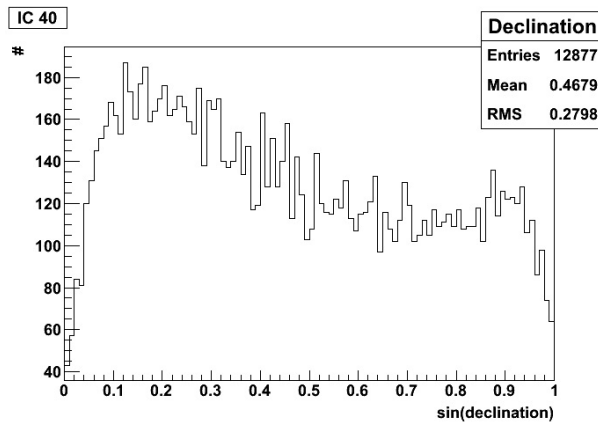


Figure 2.16: Distribution of the sine of the declination of the events

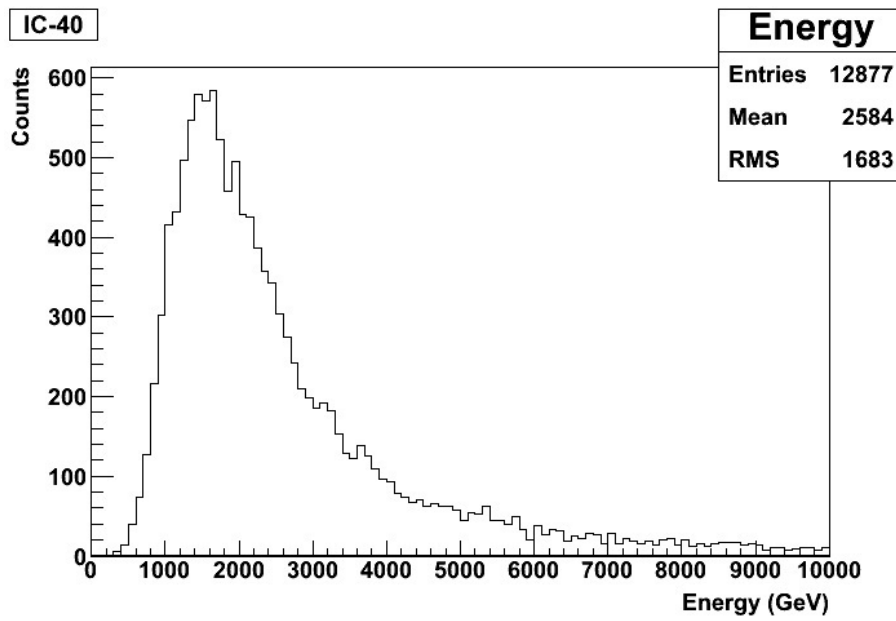


Figure 2.17: Distribution of estimated neutrino energies for our final sample.

Chapter 3

Source Stacking Analysis

Steady source candidates of cosmic rays and high-energy neutrinos are the jets of Active Galactic Nuclei. An AGN that has one of its jets pointed towards the earth is called a Blazar. As such, Blazars are the prime AGN candidates to search for related neutrino production. Out of an online blazar catalogue [5] we selected the 10 with the lowest redshift, corresponding to the 10 closest ones. We investigate a 5° window around the blazar position, because the angular resolution of IceCube is around 1° so that this window corresponds to 5σ and as such contains basically all signal events. However, the (uniform) background of atmospheric neutrinos and misreconstructed downgoing muons is largely reduced by restricting ourselves to this angular region. In IceCube we are confronted with a very low signal rate. A source stacking analysis can provide a signal identification even in these circumstances because of its cumulative nature. The recorded events of the 10 selected windows are combined in a so called “stacked window” according to their direction w.r.t. the corresponding AGN position, defined as the center of the stacked window. In case of pure background, the events in this stacked window will be distributed according to solid angle coverage due to the homogeneous character of the background. A signal however, will show up as a concentration of events at the center of the window. Consequently, we have to find a way to quantify our belief whether a stacked window exhibits a signal or not.

3.1 Bayesian degree of belief

Consider propositions A and B with prior information I and the notation $p(A|BI)$ that represents the “probability that proposition A is true in the case that proposition B and prior information are true”. In this notation the

theorem of Bayes [4] reads:

$$p(B|AI) = p(B|I) \frac{p(A|BI)}{p(A|I)} \quad (3.1)$$

This theorem is very useful for hypothesis testing. Consider hypothesis H, data D, prior information I and an unspecified alternative hypothesis H* to H. Equation 3.1 then directly yields:

$$\frac{p(H|DI)}{p(H^*|DI)} = \frac{p(H|I)}{p(H^*|I)} \frac{p(D|HI)}{p(D|H^*I)} \quad (3.2)$$

We will make use of the more intuitive decibel notation by defining the evidence of H w.r.t. H*:

$$e(H|DI) \equiv 10 \log_{10} \left(\frac{p(H|DI)}{p(H^*|DI)} \right) \quad (3.3)$$

With this notation (3.2) becomes:

$$e(H|DI) = e(H|I) + 10 \log_{10} \left(\frac{p(D|HI)}{p(D|H^*I)} \right) \quad (3.4)$$

Where $e(H|I) = 10 \log_{10} \left(\frac{p(H|I)}{p(H^*|I)} \right)$ being the prior evidence of H w.r.t. H*. To quantify the degree to which the data support a certain hypothesis H, we introduce the Bayesian observables

$$\Psi \equiv -10 \log_{10} p(D|HI) \quad (3.5)$$

$$\Psi^* \equiv -10 \log_{10} p(D|H^*I) \quad (3.6)$$

From equation (3.4) it now follows that:

$$e(H^*|DI) = e(H^*|I) + \Psi - \Psi^* \quad (3.7)$$

Since the value of a probability is a real number between 0 and 1, we always have $\Psi \geq 0$ and $\Psi^* \geq 0$. So

$$e(H^*|DI) \leq e(H^*|I) + \Psi \quad (3.8)$$

This means there is no alternative for H which can be supported by data D by more than Ψ decibel, relative to H. So the value Ψ provides the reference to quantify our degree of belief in H.

3.2 Bayesian evaluation of histogram contents

After performing our analysis we can construct a histogram containing the distribution of the angular differences of our reconstructed muon tracks w.r.t. the corresponding AGN position. Determination of the corresponding Ψ value for a pure background hypothesis will allow us to put a quantified belief in having observed a signal or only background. For this we follow the procedure of [2] to work out a scenario to determine the Ψ value for the n entries distributed over the m bins of a histogram in the light of a certain hypothesis H .

An event will fall into one of the m bins of the stacked histogram, which is equivalent to performing an experiment with m possible outcomes $\{A_1, A_2, \dots, A_m\}$. These experiments, in case all probabilities p_i corresponding to all possible outcomes A_i on successive trials are independent and stationary, belong to a so called Bernoulli class B_m [4]. Our data recordings under the hypothesis of a homogeneous background satisfy the requirements of B_m . The probability of observing n_k occurrences of each outcome A_k after n trials, $p(n_1 n_2 \dots n_m | B_m)$, is therefore given by the multinomial distribution. So the probability for observing a specific set of background data D consisting of n entries is given by:

$$p(D|B_m I) = \frac{n!}{n_1! \dots n_m!} p_1^{n_1} \dots p_m^{n_m} \quad (3.9)$$

With this knowledge and equation (3.5) we obtain an exact expression for Ψ of a (stacked) histogram:

$$\Psi = -10[\log_{10} n! + \sum_{k=1}^m (n_k \log_{10} p_k - \log_{10} n_k!)], \quad (3.10)$$

where n is the total number of entries, m is the number of bins, n_k is the number of entries in bin k and p_k is the probability for an entry to fall in bin k . For the current analysis we are dealing with a homogeneous background hypothesis and consequently the probabilities are consistent with the solid angle effect within our 5° cone:

$$p_k = \frac{1}{1 - \cos(5^\circ)} \{\cos(\Delta b \cdot k) - \cos(\Delta b \cdot [k + 1])\}, \quad (3.11)$$

where Δb is the binsize. It should be noted that this procedure is in principle independent of the binsize, since this is automatically taken into account by the corresponding p_k . However, the bin size obviously should be small enough in order not to wash out a possible signal by background.

Blazar Name	Right Ascension	Declination	Redshift
BZUJ1148+5924	177.20983	59.41567	0.011
BZUJ0048+3157	12.19642	31.95697	0.015
BZUJ0319+4130	49.95067	41.51169	0.018
BZUJ0319+4130	107.39246	50.18225	0.02
BZUJ0153+7115	28.35771	71.25181	0.022
BZUJ1719+4858	259.81025	48.98042	0.024
BZUJ1632+8232	248.13321	82.53789	0.025
BZUJ1715+5724	258.84579	57.41119	0.027
BZUJ1755+6236	268.95183	62.61225	0.027
BZBJ1104+3812	166.11379	38.20883	0.03

Table 3.1: The selected blazars from the catalogue [5] as neutrino sources for the source stacking analysis

3.3 The Ψ -analysis with IC-40 data

Using equations (3.10) and (3.11) we now have a way to calculate the Ψ -value of an experimental distribution w.r.t. a homogeneous background hypothesis. To determine whether our observations are consistent with pure background we generated 10^6 random histograms consistent with probabilities (3.11) and with the same number of entries n as for our actual measurement. Of each of these random histograms, the Ψ -value is calculated, from which we can make a distribution of the Ψ -values corresponding to background. Subsequently we determine the p-value, which is the fraction of background Ψ -values that are larger than the observed Ψ -value. To claim a signal discovery, the p-value has to be smaller than $3 \cdot 10^{-7}$ which corresponds to a 5σ effect.

To perform the source stacking analysis, we use the data of the muon neutrino candidate events recorded by the 40 string configuration of IceCube (IC 40) operated during the season 2008-2009. We also selected the 10 Blazars, listed in table 3.1, out of an online catalogue [5] based on their redshift and on their positions, to avoid overlaps, in the Northern hemisphere.

Next we investigated each source individually and selected the events within a 5° window around the source position. The 5° search area implies selecting all events within the 5σ angular uncertainty of IceCube, so 99.99994% of all the neutrino signals coming from the source are contained within the cone. Here it should be noted that the uncertainty on the AGN positions is less than an arcsecond.

Figure 3.1 is an example of the distribution of the events within a 5° window around a certain blazar. Note that the number of entries for this blazar agrees very well with the solid angle fraction (0.0038) of the Northern

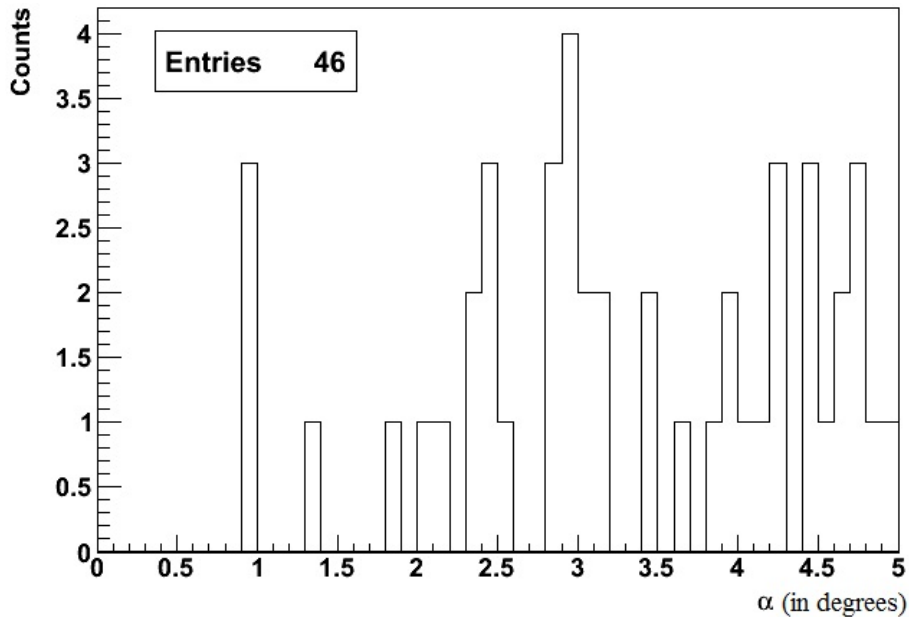


Figure 3.1: Angular distribution of events within a 5 degree cone of Blazar BZUJ1148+5924, with α the angle between the direction of the Blazar and the reconstructed track.

hemisphere atmospheric neutrinos at final analysis level (see table 2.2). We did this for all 10 sources of table 3.1 and combined all the measurements in a so called stacked histogram.

The stacked result is given in figure 3.2. It is seen that the geometrical effect, as discussed before, is in play here. The Ψ -value that corresponds with this distribution is $\Psi_{Histo} = 456.57$, which is calculated via equations (3.10) and (3.11) with $n = 407$ and $m = 50$.

To quantify our belief that the stacked histogram represents only background, we determined the p-value of Ψ_{Histo} , which is about 0.87. The Ψ -distribution of 10^6 simulated background experiments is given in figure 3.3.

From this result we conclude that we cannot claim the presence of a signal. Consequently we will proceed to give an upper limit on the signal strength.

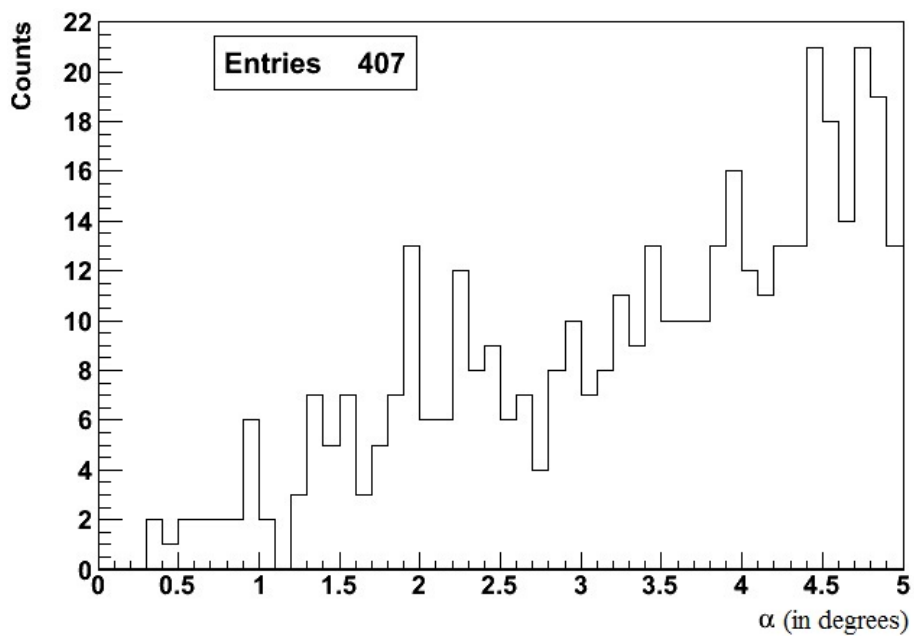


Figure 3.2: The stacked distribution of events within a 5 degree cone of all our 10 Blazars of table 3.1, with α the angle between the corresponding Blazar and the reconstructed track

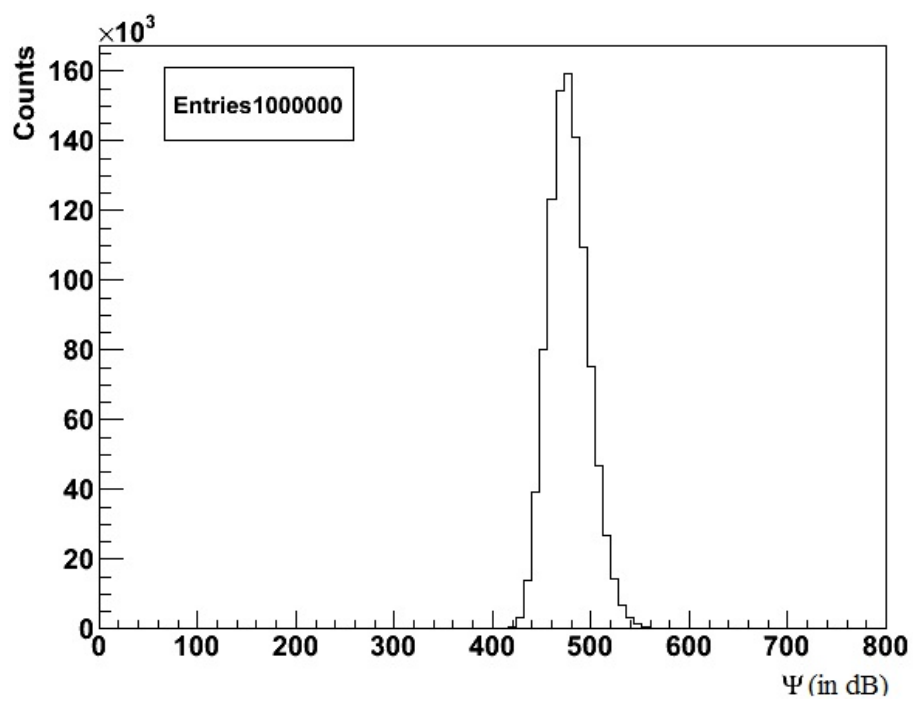


Figure 3.3: The distribution of Ψ -values of 10^6 generated background experiments

Chapter 4

Bayesian Evaluation of the Astronomical Source Strength

To provide an upper limit on the source strength, a certain patch on the sky (in this thesis a 5° window around a known AGN) is investigated over a time interval Δt with n detected neutrinos. Based on the knowledge that both background and signal events appear at a constant rate, the probability density function for the number of observed neutrinos n is given by the Poisson distribution with constant rate r :

$$p(n|rI) = \frac{(r\Delta t)^n e^{-r\Delta t}}{n!} \quad (4.1)$$

However, what we want is the rate r , so $p(r|nI)$, which can be obtained by the use of Bayes' theorem [4]:

$$p(H|DI) = p(H|I) \frac{p(D|HI)}{p(D|I)} \quad (4.2)$$

This follows from the product rule $p(HD|I) = p(H|I)p(D|HI) = p(D|I)p(H|DI)$. Using our n observed neutrinos as D , the rate r as H and the above described prior information I , this yields:

$$p(r|nI) = p(r|I) \frac{p(n|rI)}{p(n|I)} \quad (4.3)$$

Where:

- $p(r|I)$: some prior pdf for the rate
- $p(n|rI)$: is the Poisson distribution (4.1)

- $p(n|I)$ is a normalisation constant that can be determined by

$$\int p(r|nI)dr = 1 \Rightarrow p(n|I) = \int p(r|I)p(n|rI)dr \quad (4.4)$$

The rate r consists of signal and background so $r = r_s + r_b$. This transforms (4.3) into:

$$p(r_s r_b | nI) = p(r_s r_b | I) \frac{p(n | r_s r_b I)}{p(n | I)} \quad (4.5)$$

Where:

- $p(n | r_s r_b I) = \frac{([r_s + r_b] \Delta t)^n e^{-[r_s + r_b] \Delta t}}{n!}$
the poisson distribution for rate $[r_s + r_b]$
- we determine $p(r_s r_b | I)$ via the product rule by two prior pdfs: $p(r_s r_b | I) = p(r_b | I) p(r_s | r_b I) = p(r_b | I) p(r_s | I)$ because the signal rate r_s is independent of the background rate r_b
- The normalisation factor is determined as before:
 $p(n | I) = \int p(r_b | I) p(r_s | I) p(n | r_s r_b I) dr_b dr_s$

The prior background pdf $p(r_b | I)$ can be determined by the amount of detected background events in an off-source region. The prior signal pdf $p(r_s | I)$ can be determined by the usual uniform or Jeffreys prior [4], and if possible by taking into account previous results. So, to summarize, given two prior pdfs $p(r_b | I)$ and $p(r_s | I)$, we can calculate $p(r_s r_b | nI)$:

$$p(r_s r_b | nI) = p(r_b | I) p(r_s | I) \frac{p(n | r_s r_b I)}{p(n | I)} \quad (4.6)$$

However, instead of $p(r_s r_b | nI)$ we want to determine the pure source rate $p(r_s | nI)$, which we can achieve thanks to marginalisation [4]:

$$p(r_s | nI) = \int p(r_s r_b | nI) dr_b \quad (4.7)$$

Once we have $p(r_s | nI)$ and the data indicate the presence of a source we can calculate the $x\%$ credible region representing the interval in which $x\%$ of the r_s lie:

$$\int_{r_{min}}^{r_{max}} p(r_s | nI) dr_s = x\% \quad (4.8)$$

with $r_{min} < \hat{r}_s < r_{max}$ and $p(r_{min} | nI) = p(r_{max} | nI)$. r_{min} and r_{max} form the boundaries of the $x\%$ credible region of the signal rate r_s around the

peak value \hat{r}_s . In case no source signal can be identified the upper limit for r_s can be extracted from $p(r_s|nI)$ in the following way:

$$\int_0^{r_{max}} p(r_s|nI) dr_s = x\% \quad (4.9)$$

Where r_{max} now is the $x\%$ credible upper limit for the signal rate r_s . We can also go from signal rate to a source flux value Φ_s . For this we just need the effective area A_{eff} , which is the observed event rate divided by the incoming flux and is determined by simulation. Once we have determined A_{eff} corresponding to our final event selection, we find:

$$\Phi_s = r_s/A_{eff} \quad (4.10)$$

$$\Rightarrow p(\Phi_s|nI) = p(r_s|nI)/A_{eff} \quad (4.11)$$

4.1 The background rate pdf

The background rate pdf can be determined from an off-source measurement. In this analysis we point the 5 degree cone away from the source and look in a 5 degree cone at a location not corresponding to any of our selected sources. It is important to only shift the azimuth angle (right ascension) and not the zenith angle (declination), because the IceCube detector efficiency is zenith angle dependent. Due to the IC-40 configuration also an azimuth angle dependence was present, which we eliminated by shifting the azimuth angle by 180° .

So an off-source measurement results in n_0 observed background events over a certain time period t_0 . With prior information I_0 .

Using the theorem of Bayes we find

$$p(r_b|n_0I_0) = p(r_b|I_0) \frac{p(n_0|r_bI_0)}{p(n_0|I_0)} \quad (4.12)$$

With:

- $p(n_0|r_bI_0) = \frac{(r_b t_0)^{n_0} e^{-r_b t_0}}{n_0!}$ the corresponding Poisson pdf.
- $p(r_b|I_0)$ is some prior pdf for the background rate
- $p(n_0|I_0) = \int p(r_b|I_0) \frac{(r_b t_0)^{n_0} e^{-r_b t_0}}{n_0!}$ being the normalisation factor

So if we choose the prior $p(r_b|I_0)$, we can calculate $p(n_0|I_0)$ and thus determine the posterior background rate pdf $p(r_b|n_0I_0)$

In this thesis we will use the following uniform background prior:

$$p(r_b|I_0) = \frac{1}{r_{bmax} - r_{bmin}} \quad (4.13)$$

Since $r_{bmin} = 0$ this becomes:

$$p(r_b|I_0) = \frac{1}{r_{bmax}}. \quad (4.14)$$

Using this prior yields:

$$p(n_0|I_0) = \int_0^{r_{bmax}} \frac{1}{r_{bmax}} \frac{(r_b t_0)^{n_0} e^{-r_b t_0}}{n_0!} dr_b \quad (4.15)$$

for the normalisation factor. To solve this integral we make use of $\int_0^x y^n e^{-y} dy = \gamma(n+1, x)$, being the incomplete gamma function [14]. This finally results in the following posterior background rate pdf:

$$p(r_b|n_0I_0) = \frac{t_0 (r_b t_0)^{n_0} e^{-r_b t_0}}{\gamma(n_0 + 1, r_{bmax} t_0)} \quad (4.16)$$

If $r_{bmax} t_0 \gg n_0$, the approximation $\gamma(n_0 + 1, r_{bmax} t_0) \approx \gamma(n_0 + 1) = n_0!$ is very usefull.

Since an event rate cannot be negative a (modified) Jeffrey's prior [4] could also be used. However, this will heavily complicate the mathematics and is beyond the scope of this thesis.

4.2 On-source rate prior pdf

The actual on-source measurement consists of n events (signal+background) over a certain time period t. Ater having performed the off-source measurement(s), we may use the obtained posterior background pdf as the prior for the background in the determination of the signal rate as outlined in equation (4.6). So we go back to equation (4.6):

$$p(r_s r_b | nI) = p(r_b | I) p(r_s | I) \frac{p(n | r_s r_b I)}{p(n | I)} \quad (4.17)$$

Where:

- $p(n | r_s r_b I)$ is a poisson pdf with rate $r_s + r_b$

- $p(r_b|I)$ and $p(r_s|I)$ are the two prior pdfs that need to be chosen
- $p(n|I)$ the normalisation factor

Once we choose the two prior pdfs $p(r_b|I)$ and $p(r_s|I)$, we automatically fix the normalisation factor $p(n|I)$ after calculating the integral and will have all the elements for $p(r_s r_b|nI)$. As background prior we use the off-source posterior pdf:

$$p(r_b|I) = \frac{t_0(r_b t_0)^{n_0} e^{-r_b t_0}}{\gamma(n_0 + 1, r_{bmax} t_0)} \quad (4.18)$$

For the $p(r_s|I)$ prior we use the uniform prior (with $r_{smin} = 0$):

$$p(r_s|I) = \frac{1}{r_{smax}} \quad (4.19)$$

Equation (4.19) leads to the following integral for the normalisation factor:

$$p(n|I) = \int_0^{r_{smax}} \int_0^{r_{bmax}} \frac{1}{r_{smax}} \frac{t_0(r_b t_0)^{n_0} e^{-r_b t_0}}{\gamma(n_0 + 1, r_{bmax} t_0)} \frac{([r_s + r_b] t_0)^n e^{-[r_s + r_b] t_0}}{n!} dr_b dr_s \quad (4.20)$$

Since our interest is in the pure source rate pdf $p(r_s|nI)$ we have to marginalise $p(r_s r_b|nI)$ by integrating over dr_b :

$$\begin{aligned} p(r_s|nI) &= \int_0^{r_{bmax}} p(r_b|I) p(r_s|I) \frac{p(n|r_s r_b I)}{p(n|I)} dr_b \\ &= \frac{\int_0^{r_{bmax}} p(r_b|I) p(n|r_s r_b I) dr_b}{r_{smax} p(n|I)} \equiv \frac{A}{B} \end{aligned} \quad (4.21)$$

We have written this ratio as A/B to split the calculation in two parts. For A we get:

$$\begin{aligned} A &= \int_0^{r_{bmax}} p(r_b|I) p(n|r_s r_b I) dr_b \\ &= \int_0^{r_{bmax}} \frac{t_0(r_b t_0)^{n_0} e^{-r_b t_0}}{\gamma(n_0 + 1, r_{bmax} t_0)} \frac{([r_s + r_b] t_0)^n e^{-[r_s + r_b] t_0}}{n!} dr_b \end{aligned} \quad (4.22)$$

And for B:

$$\begin{aligned}
B &= r_{smax} p(n|I) \\
&= \int_0^{r_{smax}} \int_0^{r_{bmax}} \frac{t_0 (r_b t_0)^{n_0} e^{-r_b t_0}}{\gamma(n_0 + 1, r_{bmax} t_0)} \frac{([r_s + r_b] t_0)^n e^{-[r_s + r_b] t_0}}{n!} dr_b dr_s \quad (4.23)
\end{aligned}$$

The factors that A and B have in common and can be put outside the integral are: $\frac{1}{\gamma(n_0 + 1, r_{bmax} t_0) n!}$, $t_0^{n_0 + 1}$ and t^n . So we can cancel these factors, which yields:

$$A = \int_0^{r_{bmax}} (r_b)^{n_0} e^{-r_b t_0} (r_s + r_b)^n e^{-(r_s + r_b)t} dr_b dr_s \quad (4.24)$$

$$\begin{aligned}
B &= \int_0^{r_{smax}} \int_0^{r_{bmax}} (r_b)^{n_0} e^{-r_b t_0} (r_s + r_b)^n e^{-(r_s + r_b)t_0} dr_b dr_s \quad (4.25) \\
&= \int_0^{r_{smax}} A dr_s
\end{aligned}$$

The first step in calculating this integral is to make use of the binomial expansion of $(r_s + r_b)^n$:

$$(r_b + r_s)^n = \sum_{i=0}^n \frac{n!}{i!(n-i)!} (r_s)^i (r_b)^{(n-i)} \quad (4.26)$$

Substituting (4.26) into (4.24) yields:

$$A = \sum_{i=0}^n \frac{n!}{i!(n-i)!} (r_s)^i e^{-r_s t} \int_0^{r_{bmax}} (r_b)^{(n+n_0-i)} e^{-r_b(t+t_0)} dr_b \quad (4.27)$$

Since $\int_0^x y^n e^{-y} dy = \gamma(n+1, x)$, we can solve the integral:

$$\begin{aligned}
A &= \sum_{i=0}^n \frac{n!}{i!(n-i)!} (r_s)^i e^{-r_s t} \frac{\gamma(n+n_0-i+1, r_{bmax}(t+t_0))}{(t+t_0)^{(n+n_0-i+1)}} \\
&= \frac{n! e^{-r_s t}}{(t+t_0)^{(n+n_0+1)}} \sum_{i=0}^n \frac{(r_s)^i (t+t_0)^i \gamma(n+n_0-i+1, r_{bmax}(t+t_0))}{i!(n-i)!} \quad (4.28)
\end{aligned}$$

Having obtained an expression for A, we can integrate it over r_s to get B:

$$\begin{aligned}
B &= \frac{n!}{(t+t_0)^{n+n_0+1}} \sum_{j=0}^n \frac{(t+t_0)^j \gamma(n+n_0-j+1, r_{bmax}(t+t_0))}{j!(n-j)!} \int_0^{r_{smax}} (r_s)^j e^{-r_s t} dr_s \\
&= \frac{n!}{(t+t_0)^{n+n_0+1}} \sum_{j=0}^n \frac{(t+t_0)^j \gamma(n+n_0-j+1, r_{bmax}(t+t_0))}{j!(n-j)!} \gamma(j+1, r_{smax}t)
\end{aligned} \tag{4.29}$$

So finally we have the pure, background independent, posterior signal rate pdf:

$$p(r_s|nI) = \frac{e^{-r_s t} \sum_{i=0}^n \frac{(r_s)^i (t+t_0)^i \gamma(n+n_0-i+1, r_{bmax}(t+t_0))}{i!(n-i)!}}{\sum_{j=0}^n \frac{(t+t_0)^j \gamma(n+n_0-j+1, r_{bmax}(t+t_0))}{j!(n-j)!} \gamma(j+1, r_{smax}t)} \tag{4.30}$$

Where n is the amount of events in the stacked on-source measurement, n_0 the amount of selected off-source events and t (t_0) the time duration of the on (off) source measurement.

As was mentioned before, we can't claim the observation of a signal. As such we will determine an upper limit on the signal strength in the next section.

4.3 Determination of the source flux upper limit

We investigated 5° windows around the 10 blazars from table 3.1, which provides us the ‘‘on source’’ stacked histogram shown in figure 3.2.

The background was determined via off-source measurements as outlined before and shown in figure 4.1.

The total number of on-source events is $n = 407$ whereas the total number of off-source events is $n_0 = 409$. The IC-40 sample has been taken over a time period of 408 days, so that both the exposures for on-source (t) and off-source (t_0) amount to 408 days. We took $r_{bmax} = \frac{n_0}{t_0} \cdot 100 = 0.00116$ Hz and $r_{smax} = 1$ Hz, which are both comfortably large enough. These values can be chosen large because there was no noticeable difference in the end result when other values were taken.

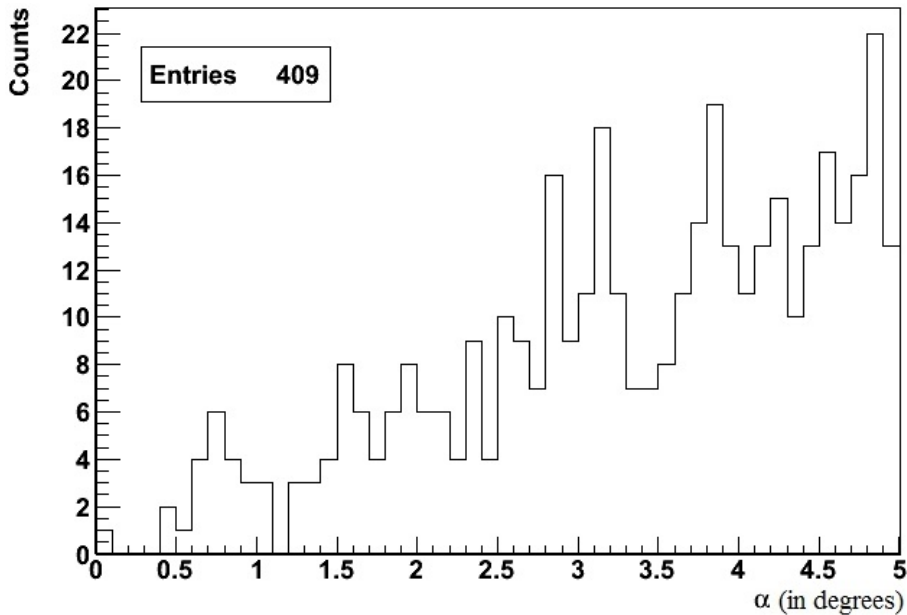


Figure 4.1: The stacked distribution of events within a 5 degree off-source background region, 180° shifted from the various blazar positions

We are now able to determine the posterior source rate pdf for a uniform prior, using (4.30). The resulting pdf is shown in figure 4.3, from which we determine the 90% upper limit r_{smax} for the signal rate r_s :

$$\int_0^{r_{smax}} p(r_s|nI)dr_s = 90\% \quad (4.31)$$

This yields $r_{smax} = 1.318 \cdot 10^{-6}$ Hz. Note that this rate doesn't take into account the reconstruction efficiency but since we are only interested in the flux this correction is not needed here. We can translate this into a flux using the effective area (see figure 4.2), which by definition takes all reconstruction efficiencies into account. For the current analysis we use the angle averaged effective area, weighted by the observed energy estimate shown in figure 4.2. The corresponding effective area is $A_{eff} = 62.49 \cdot 10^5$ cm² and our analysis was performed on 10 patches of 5° around a source, representing in total 0.038 sr which leads to a 90 % upper limit for the signal flux of $\Phi_{\nu_\mu}^{ul} = \frac{r_{smax}}{A_{eff} \cdot 0.038} = 5.82 \cdot 10^{-12}$ s⁻¹cm⁻²sr⁻¹. However, this flux upper limit doesn't take into account the effect of neutrino oscillations. At the source we have (see figure 1.4) $\nu_\mu : \nu_e : \nu_\tau = 2:1:0$. Assuming maximum oscillation we will observe on the Earth $\nu_\mu : \nu_e : \nu_\tau = 1:1:1$. A tiny fraction of the ν_τ will produce a muon which might also be detected in iceCube. However, we

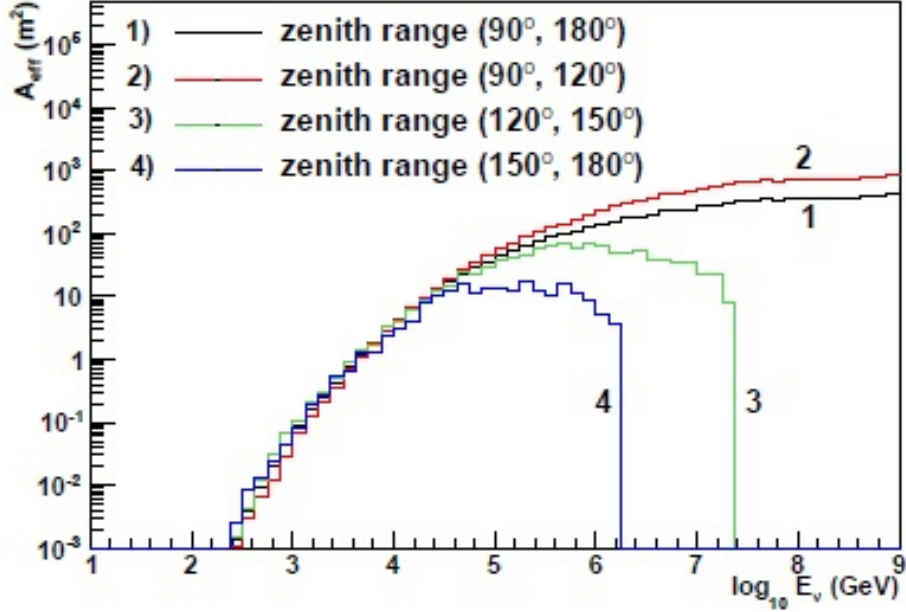


Figure 4.2: Effective Area for $\nu_\mu + \bar{\nu}_\mu$ as a function of the true neutrino energy in intervals of the true zenith angle of the neutrino. The angle averaged area is represented by the solid black line.

will neglect this effect since it would need a special ν_τ simulation which is beyond the scope of this thesis. So our final value for the 90% upper limit for a signal flux is $\Phi_{\nu_\mu}^{ul} = 11.64 \cdot 10^{-12} \text{ s}^{-1} \text{ cm}^{-2} \text{ sr}^{-1}$, as compared to the value of a previous analysis: $\Phi_{mean}^{ul} = 8.89 \cdot 10^{-12} \text{ s}^{-1} \text{ cm}^{-2} \text{ sr}^{-1}$ [6].

We thus see that the flux determined by this method using the 10 selected sources, agrees well with the previous method [6] which investigated the diffuse flux of the complete Northern hemisphere. The Bayesian method provided us with an analytic expression for the source rate pdf, which can be integrated to the exact upper limit value desired. As such there is no oversampling problem as in the Feldman-Cousins method [15] used in [6], which can introduce significant effects in the tail of the pdf.

Our Bayesian approach introduces a learning process that can make use of previously determined results, independently of the method by which they were obtained.

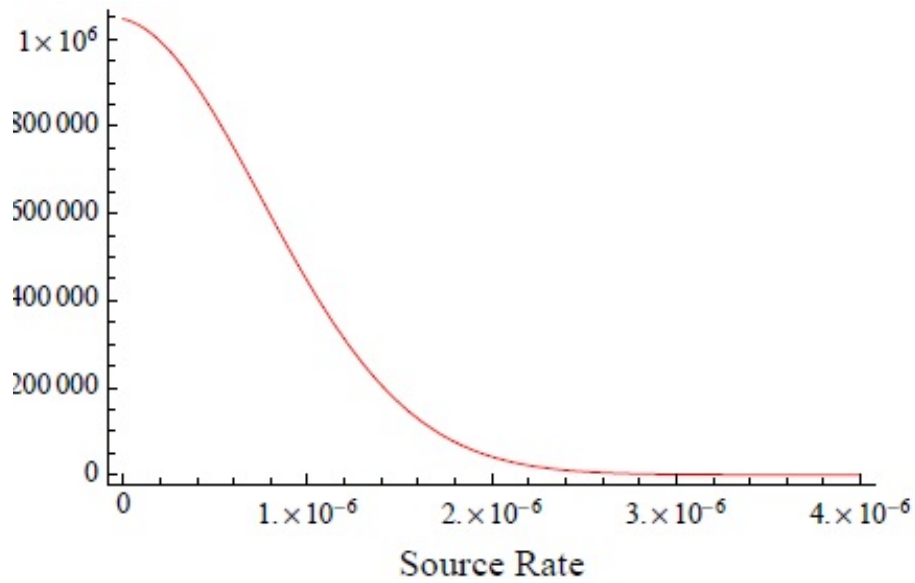


Figure 4.3: The posterior source rate pdf, calculated using the observations mentioned in the text and equation (4.30)

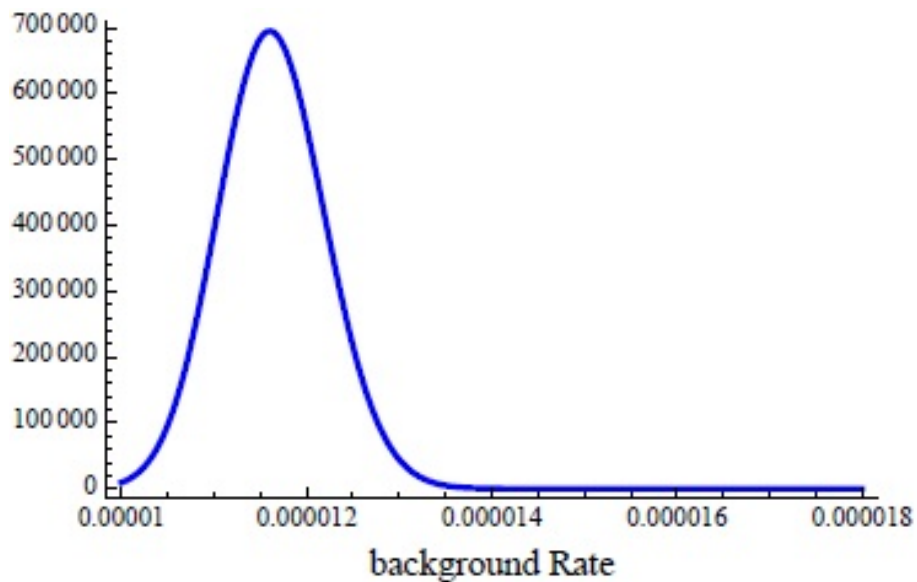


Figure 4.4: The posterior background rate pdf, calculated using the observations mentioned in the text and equation (4.16)

Chapter 5

Summary and outlook

5.1 Summary

IceCube is a neutrino telescope built at the South Pole. It is essentially an array of Digital Optical Modules positioned in an 1 km^3 ice volume. It detects neutrinos indirectly by detecting the cherenkov light of the leptons that are formed when the neutrino interacts with the ice volume or the bedrock below it. IceCube has to deal with a huge amount of background coming from atmospheric muons. The different levels of the performed event selections are discussed, which have all been determined by finding a compromise between remaining as much signal as possible while removing as much background as possible. The selected data set that remains after all this processing, forms the starting point of this thesis.

Previously this dataset has been analysed by a frequentist method to look for a diffuse flux of high-energy neutrinos coming from astrophysical sources. No significant flux was found by this method and an upper limit for the signal strength was determined using a Feldman-Cousins method. In this thesis we analyse the data using a Bayesian method, which consists of two parts.

First, we performed a source stacking analysis which quantifies our belief in the presence of a source by making use of Bayes' theorem. This analysis looks in the direction of known sources of interest, which consists of 10 AGN selected from an online catalogue in this thesis. We proceed by selecting all the events within a 5° window of the individual directions of each of the selected AGN. Next we "stack" these windows upon each other which makes this method more sensitive for weaker signals, from which we construct a declination histogram, see fig. 3.2. The Bayesian observable Ψ is introduced (starting from the theorem of Bayes) and applied to quantify our belief to whether the histogram supports the presence of a source (equations 3.10 and

3.11). From this Ψ -value we determine the corresponding p-value by generating 10^6 random histograms, calculating the Ψ -value of each and eventually constructing the Ψ -distribution. This resulted in a $p=0.87$, meaning 87% of the randomly generated histograms have a Ψ -value larger than our stacked sources histogram. From this result we conclude that we cannot claim the presence of a signal source in our selected AGN.

Second, we proceed by determining the upper limit on the source strength in a Bayesian way. Starting from the theorem of Bayes, we arrive at equation (4.17):

$$p(r_s r_b | nI) = p(r_b | I) p(r_s | I) \frac{p(n | r_s r_b I)}{p(n | I)}$$

Where:

- $p(n | r_s r_b I) = \frac{([r_s + r_b] \Delta t)^n e^{-[r_s + r_b] \Delta t}}{n!}$
the poisson distribution for rate $[r_s + r_b]$
- $p(r_b | I)$ and $p(r_s | I)$ the two priors that need to be chosen
- The normalisation factor is determined as before:
 $p(n | I) = \int p(r_b | I) p(r_s | I) p(n | r_s r_b I) dr_b dr_s$

For the on-source signal prior $p(r_s | I)$, we chose a uniform distribution (4.19) and for the on-source background prior $p(r_b | I)$ we used the off-source posterior prior (4.18). By substituting this into equation (4.17) and by making use of marginalisation, we can calculate the pure, background independent, posterior signal rate pdf which resulted in equation (4.30):

$$p(r_s | nI) = \frac{e^{-r_s t} \sum_{i=0}^n \frac{(r_s)^i (t + t_0)^i \gamma(n + n_0 - i + 1, r_{bmax}(t + t_0))}{i!(n - i)!}}{\sum_{j=0}^n \frac{(t + t_0)^j \gamma(n + n_0 - j + 1, r_{bmax}(t + t_0))}{j!(n - j)!} \gamma(j + 1, r_{smax} t)}$$

The experimental values that we have to substitute into (4.30) are the number of signal events n , the number of background events n_0 and the live times t and t_0 . These are determined by two different experiments (making use of the same data set): an on-source experiment looking at the sources and an off-source experiment looking at background regions. This resulted in $n=407$, $n_0=409$ and equal live times t and t_0 . Armed with these results we can calculate the posterior signal rate pdf (4.30).

This posterior signal rate pdf is then integrated to a r_{smax} value that corresponds with a 90% upper limit. Taking the effective area (= observed event rate/incoming flux) into account and the fact that this analysis covers 0.038 sr, we get the following 90% upper limit for the signal flux: $\Phi_{\nu_\mu}^{ul} = 11.64 \cdot 10^{-12} \text{ s}^{-1}\text{cm}^{-2}\text{sr}^{-1}$, which includes the effect of neutrino oscillations.

The resulting flux that comes out of this novel method, is in nice agreement with the previously determined flux [6]. Due to our limited amount of sources we investigated only a small fraction of the Northern hemisphere (versus the whole hemisphere in the previous method) which leads to a less stringent flux limit.

5.2 Outlook

The next step for this analysis can be performed with the complete IceCube detector, which will yield a better resolution. Two ways to improve the statistics is by selecting more sources to investigate and by prolonging the live time of the observations using the full IceCube detector.

The method itself can be improved by using a more sophisticated prior, like a Jeffrey's prior instead of a uniform prior as was done in this thesis. Also the small fraction of ν_τ that induce a detectable muon track in the detector can be taken into account in a future analysis, as well as a study of the various sources of systematic uncertainties.

Bibliography

- [1] IceCube Collaboration *An absence of neutrinos associated with cosmic-ray acceleration in γ -ray bursts* Nature 484, 351-354 (19 April 2012)
- [2] N. Van Eijndhoven, *On the observability of high-energy neutrinos from gamma ray bursts*, Astropart. Phys. 28, (2008) 540546
- [3] E. Waxman and J. Bahcall, Phys. Rev. Lett. 78: 2292-2295 (1997)
- [4] Edwin T. Jaynes, G. Larry Bretthorst *Probability Theory: The Logic of Science*, Cambridge University Press, 2003
- [5] <http://www.asdc.asi.it/bzcat/>
- [6] R. Abasi, et al., *A search for a Diffuse Flux of Astrophysical Muon Neutrinos with the IceCube 40-String Detector*, arXiv:1104.5187v4
- [7] R. Abbasi, et al., Nucl. Instr. and Meth. A 601 (2009) 294-316
- [8] J. Ahrens et al., Astropart. Phys. 20 (2004) 507-532.
- [9] R. Abbasi et al., Nucl. Inst. Meth. A (2011),
- [10] J. Ahrens, et al., Nucl. Instr. and Meth. A524 (2004) 169
- [11] T. Neunh"offer, *Estimating the angular resolution of tracks in neutrino telescopes based on a likelihood analysis*, 2004, arXiv:astro-ph/0407044v1
- [12] N. van Eijndhoven et al., Astropart. Phys. 28 (2007) 456
- [13] F. James, minuit: Function minimalisation and error analysis, CERN report D506, (1994). <http://wwwasdoc.web.cern.ch/wwwasdoc/minuit>
- [14] *Numerical Recipes 3rd Edition: The Art Of Scientific Computing*, William H. Press, Saul A. Teukolsky, William T. Vetterling and Brian P. Flannery, Cambridge University Press

[15] G.J. Feldman and R.D. Cousins, Phys. Rev. **D57** (1998) 3873